DOE/JPL-956786-86/2
9950-1229

Development of High-Efficiency Solar Cells on Silicon Web

D. L. Meier, J. Greggi, T. W. O'Keeffe, and P. Rai-Choudhury

Eighth Quarterly Progress Report
January 1 to March 31, 1986
Contract No. 956786

This work was performed for the
Jet Propulsion Laboratory

May 12, 1986

Westinghouse R&D Center
1310 Beulah Road
Pittsburgh, Pennsylvania 15235

This report was prepared for the Jet Propulsion Laboratory, California Institute of Technology, sponsored by the National Aeronautics and Space Administration.

Development of High-Efficiency Solar Cells on Silicon Web

D. L. Meier, J. Greggi, T. W. O'Keeffe, and P. Rai-Choudhury

Eighth Quarterly Progress Report
January 1 to March 31, 1986
Contract No. 956786

This work was performed for the
Jet Propulsion Laboratory

May 12, 1986

Westinghouse R&D Center
1310 Beulah Road
Pittsburgh, Pennsylvania 15235

NOTICE

For the sake of completeness, results have been included in this report which were obtained with support from the Electric Power Research Institute (EPRI) under Partial Order Transfer 54-7-RLC-401319 from the Westinghouse Advanced Energy Systems Division to the Westinghouse R&D Center.

CONTENTS

LIST OF FIGURES

LIST OF TABLES

1. SUMMARY

The major objective of this contract is to improve web base material with a goal of obtaining solar cell efficiencies in excess of 18% (AM1). Efforts in this program are directed toward identifying carrier loss mechanisms in web silicon, eliminating or reducing these mechanisms, designing a high-efficiency cell structure with the aid of numerical models, and fabricating high-efficiency web solar cells. Fabrication techniques must preserve or enhance carrier lifetime in the bulk of the cell and minimize recombination of carriers at the external surfaces.

During this reporting period, three completed cells were viewed by cross-sectional TEM in order to investigate further the relation between structural defects and electrical performance of web cells. Consistent with past TEM examinations, the cell with the highest efficiency (15.0%) had no dislocations but did have 11 twin planes. Of the remaining two cells, one was made from a section near the beginning of a crystal and the other was made from a section near the end of the same crystal. The most prominent feature of this pair of cells is the location of the twin planes relative to the external surface. For the cell near the beginning of the crystal, the heavily twinned region is located approximately midway through the thickness of the web. For the cell near the end of the crystal, the heavily twinned region has moved to within a few microns of the external surface. This suggests that the termination of the crystal may have been a result of the twin planes exiting the web ribbon.

In order to passivate the dislocation/precipitate structural defect that has been observed by TEM in completed web cells, hydrogen

ions have been implanted into web strips. The implantation was done after boron and phosphorus diffusions, but before metallization. This is the first time that hydrogen has been implanted at this point in the processing sequence. Implanting hydrogen at this point is compatible with the overall Westinghouse process.

Results for small area (1 cm^2) web cells were very encouraging. For example, a web cell without hydrogen implantation had an electron diffusion length of 19 μm and an efficiency of 11.9%. With hydrogen implantation, the diffusion length and efficiency of a corresponding cell improved to 120 μm and 16.1%, respectively. It was also found that web cells which had a high efficiency without hydrogen implantation (16.7%) were not improved further by the implant. Presumably, this is because there were very few defect levels to passivate in this superior quality web material.

An attempt was also made to passivate a number of full-sized (2.0 x 9.8 cm) cells. In this case, the improvement was less pronounced than for the small (1 cm^2) cells. This may be a consequence of non-uniformity of the ion beam or of insufficient temperature rise of the web strip during implantation. These factors are being investigated, and a second trial with full-sized web cells will be made.

Finally, web cells 2 x 2 cm in size have been fabricated with oxide-passivated front and back surfaces, an aluminum back surface reflector, and a double-layer (ZnS and MgF_2) antireflective coating. The web substrate resistivity was nominally 4 ohm-cm, and the cell thickness was approximately 130 μm. The best web cell had an efficiency of 16.5%, with a short-circuit current density of 37.5 mA/cm^2 and an electron lifetime of 38 μs as measured by the open-circuit voltage decay (OCD) technique. For comparison, cells using Wacker float zone (0.2 ohm-cm) substrates were also fabricated as controls. The best float zone cell had an efficiency of 18.3% with a short-circuit current

density of 35.9 mA/cm^2 and an OCD lifetime of 18 μs. It is interesting to note that the best web cell was superior in short-circuit current and lifetime to the best float zone cell. However, the lower resistivity of the float zone material resulted in higher values of open-circuit voltage and fill factor, and hence in higher efficiency than the web cell. Future plans call for using low-resistivity (0.2 ohm-cm) web substrates along with hydrogen implantation in order to approach the efficiency presently obtainable with low-resistivity float zone substrates (18%).

A total of eight web cells, all 2 x 2 cm in size, have been delivered to JPL as required by the contract. This is the first time that cells 4 cm^2 in area have been fabricated with the "high-efficiency" process; previously, only cells 1 cm^2 in area were fabricated. The cells were accompanied by measurement results, including lighted I-V, quantum efficiency, and minority carrier lifetime.

2. INTRODUCTION

The idealized efficiency of a silicon solar cell is about 25%, although present day cells fall considerably short of this limiting value. This is largely a consequence of heavy doping effects, nonideal bulk parameters (particularly minority carrier diffusion length), and a high rate of recombination at the cell surfaces. The major problems of efficiency improvements fall in the above categories. In addition, efficient contacts and antireflective coatings are essential and must be optimized consistent with device structure.

Starting material is vitally important for high-efficiency cells, since high efficiency (>18%) cannot be realized if the starting material is poor or if it degrades with processing. The objective of this program is to understand and improve web silicon so that high-efficiency web cells can be fabricated using advanced cell design and processing. This includes the understanding of mechanisms which limit the diffusion length in web silicon, the development of means for eliminating or ameliorating these mechanisms, the recognition of excessive recombination activity in all regions of an operating cell, and the reduction of this recombination.

This eighth quarterly report describes the results of a continuing transmission electron microscopy (TEM) investigation to understand better the extended structural defects that exist in web material, the results of low-energy high-dose hydrogen ion implantation to passivate these defects, and the results of advanced processing to fabricate high-efficiency web cells.

3. TECHNICAL PROGRESS

3.1 CROSS-SECTIONAL TEM VIEWS OF THREE WEB CELLS

Three additional web cells were examined by cross-sectional TEM. The web substrate for cell 21B was grown from the R-furnace, which often produces material from which cells of very good quality are made. This cell was examined to aid in further clarifying the characteristics of good cells and good material. Cells 8B and 17B were made from the same crystal, one near the beginning of the crystal (8B) and the other from near the end of the crystal (17B). The purpose for examining this pair of cells is to see if any significant difference exists between the material at the extremes of a web crystal.

Figures 1 and 2 show the results for cell 21B, which had an efficiency of 15.0%, and which was made from crystal R-492-15.5. Note that there are 11 twin boundaries distributed over 3.6 μm in depth and that there are very few dislocations, either in the heavily twinned region or in the bulk. This is consistent with earlier results which showed that a high efficiency (15.0%) results from material with few dislocations, in spite of the reasonably large number of twin planes (11). Again, the twin planes, themselves, do not seem to play a role in limiting the efficiency of the cells. The diffusion length for this cell, measured by the surface photovoltage technique, was 137 μm.

Figures 3 and 4 show the results for cell 8B, which was fabricated from section 2 of crystal 2-297-16. The efficiency of this cell was 14.0%, and section 2 was within 66 cm of the beginning of the crystal. There are 21 twin boundaries distributed over a 3.9 μm depth, and the twin boundaries are located approximately midway through the thickness of the crystal. Dislocations were evident both in the heavily twinned region (1.3×10^{7} cm^{-2}) and in the bulk of the cell.

CELL 21B:R492-15.5:(15%)

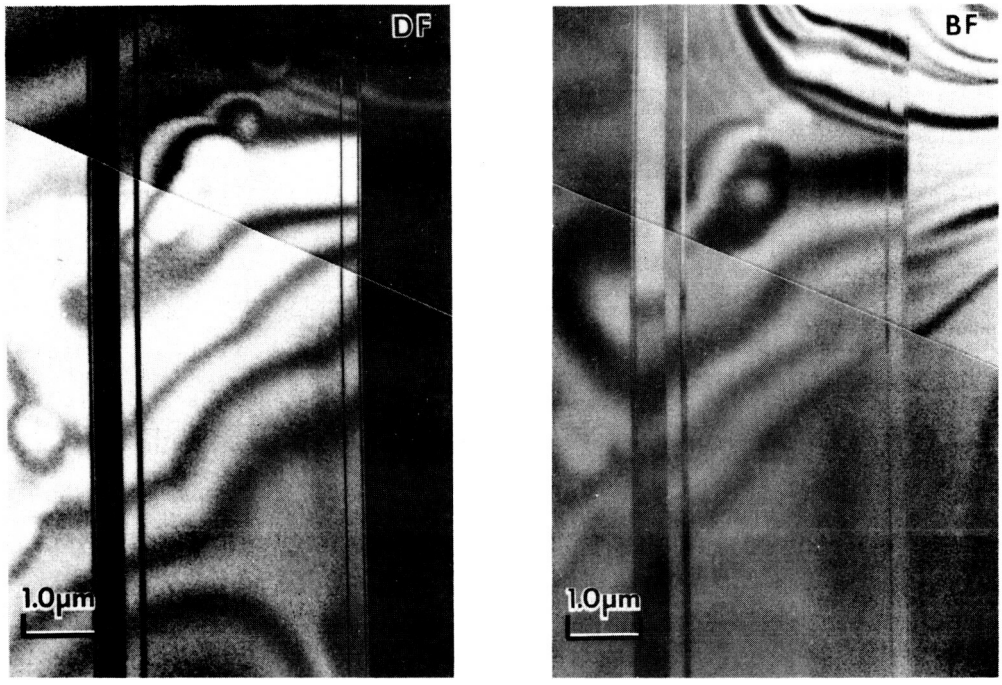

Twin Planes Vertical

Figure 1 — Cross-sectional TEM view of cell 21B (15%) from furnace R showing 11 twin boundaries distributed over 3.6 μm in depth.

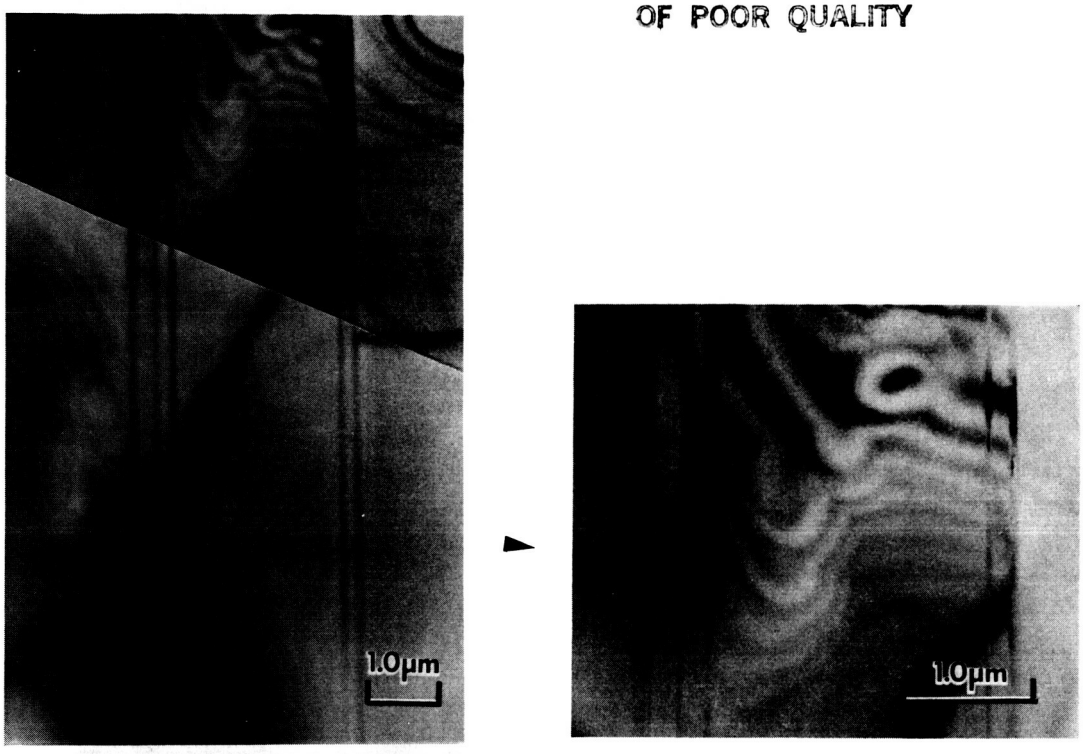

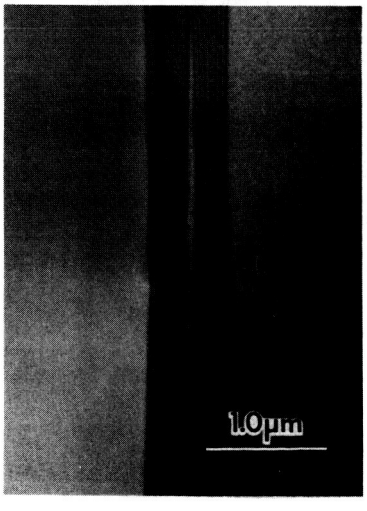

CELL 21B:R492-15.5:(15%)

Twin Planes Tilted

Figure 2 — Cross-sectional TEM view of cell 21B with twin planes tilted showing only an occasional dislocation.

CELL 8B:2297-16.2:(14%)

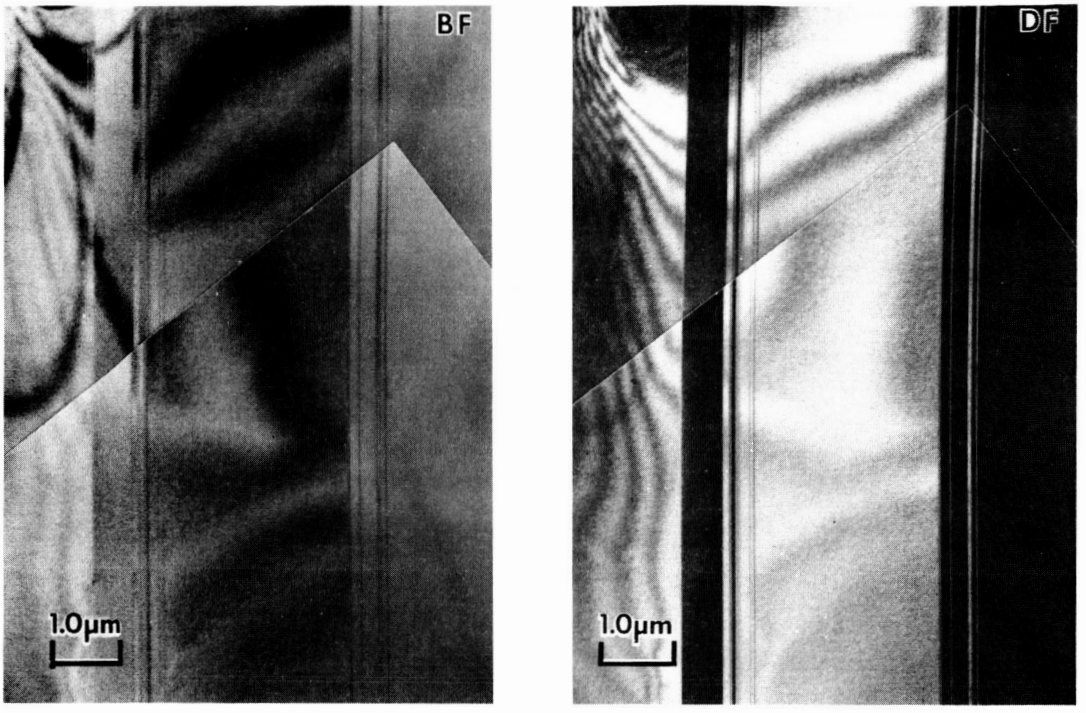

Twin Planes Vertical

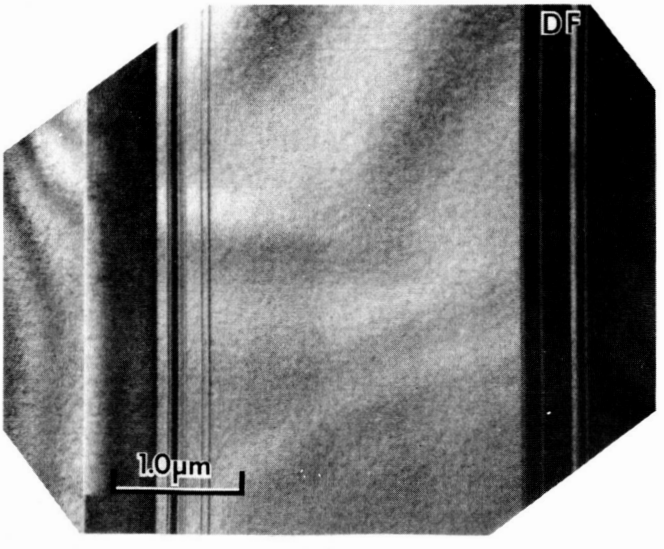

Figure 3 — Cross-sectional TEM view of cell 8B (14%) from section 2 of crystal 2-297-16 showing 21 twin boundaries distributed over 3.9 μm in depth.

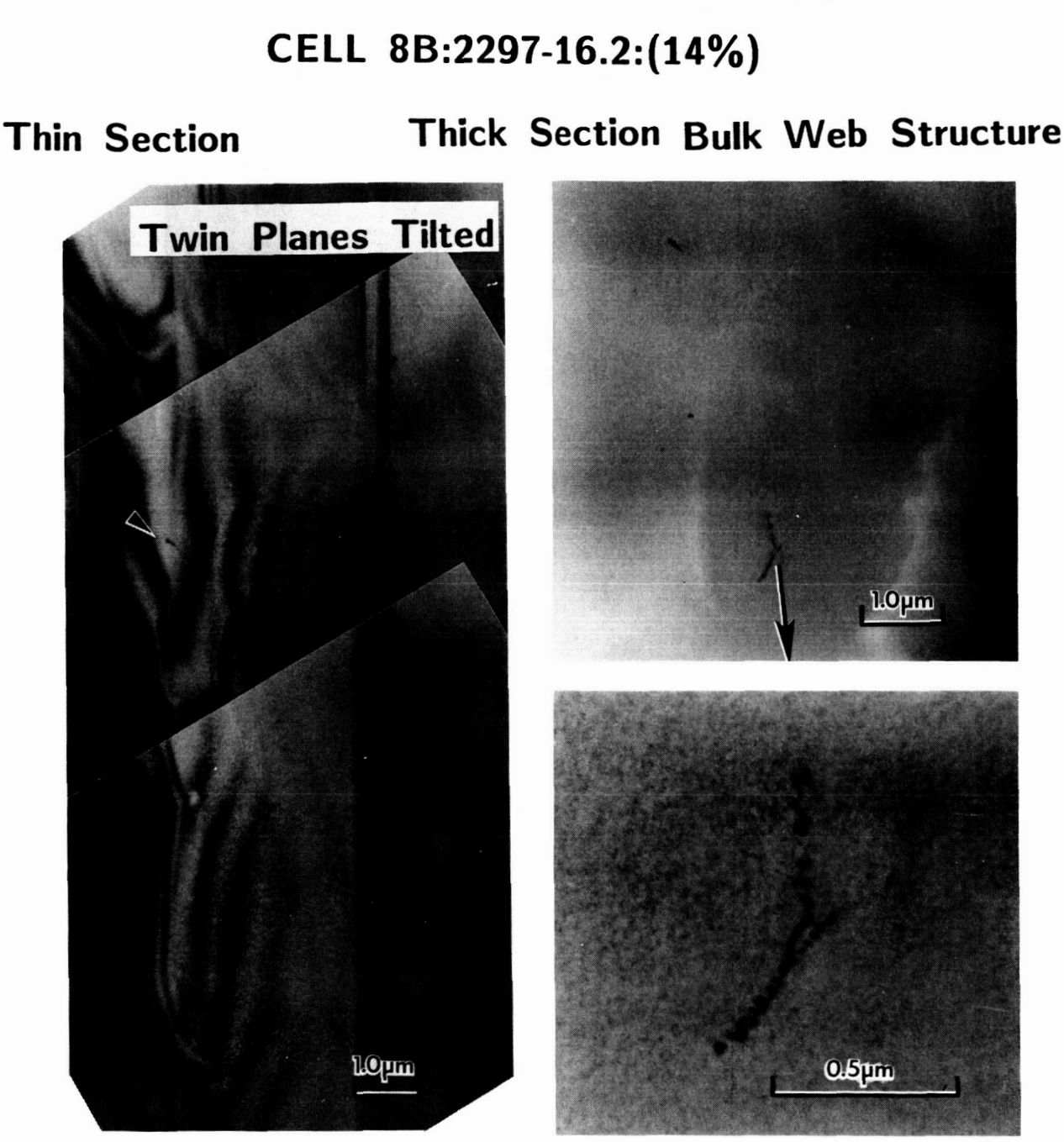

Figure 4 — Cross-sectional TEM view of cell 8B with twin planes tilted showing dislocations piled up at the twin planes (1.3×10^7 dislocations/cm^2) and also in bulk.

Figures 5, 6, and 7 show the results for cell 17B, which was fabricated from section 14 of crystal 2-297-16. Section 14 was approximately 460 cm from the beginning of the crystal and was the last section of the crystal before it terminated. (This crystal was also a part of the 27,000 cm^2 growth run which first demonstrated web weekly throughput exceeding 25,000 cm^2.) The efficiency of this cell was 12.9%, a decrease from the 14.0% value of cell 8B above. There were 13 twin boundaries distributed over 3.3 μm in depth. Dislocations were present at a higher concentration in the heavily twinned region (3.6×10^7 cm^{-2}) than for cell 8B and were also found in the bulk.

The most striking feature of the TEM views for cell 17B is that the heavily twinned region is very close to the external surface of the web. Figure 5 shows that only 2.6 μm separates the external surface of the crystal from the beginning of the heavily twinned region. This suggests that the cause for termination of this crystal may have been the movement of the twinned region to the external surface. It is also possible that the lower efficiency of this cell, compared to cell 8B, is associated with having the heavily twinned region quite close to the external surface. If this surface was the front of the cell, then the relatively high density of dislocations in the heavily twinned region would be expected to degrade the cell efficiency.

3.2 HYDROGEN ION IMPLANTATION INTO WEB CELLS AFTER DIFFUSIONS USING THE WESTINGHOUSE SYSTEM

It has been demonstrated that silicon web can be grown and processed with a dislocation density that is below the detection limit of TEM, and that with such material it is possible to fabricate cells with efficiencies exceeding 15% by the baseline processing sequence at Westinghouse AESD.[1] However, the growth conditions are not sufficiently well controlled as yet to produce, at will, web material in which the diffusion length approaches the thickness. Since such superior quality material is required in order to meet the efficiency objectives of this

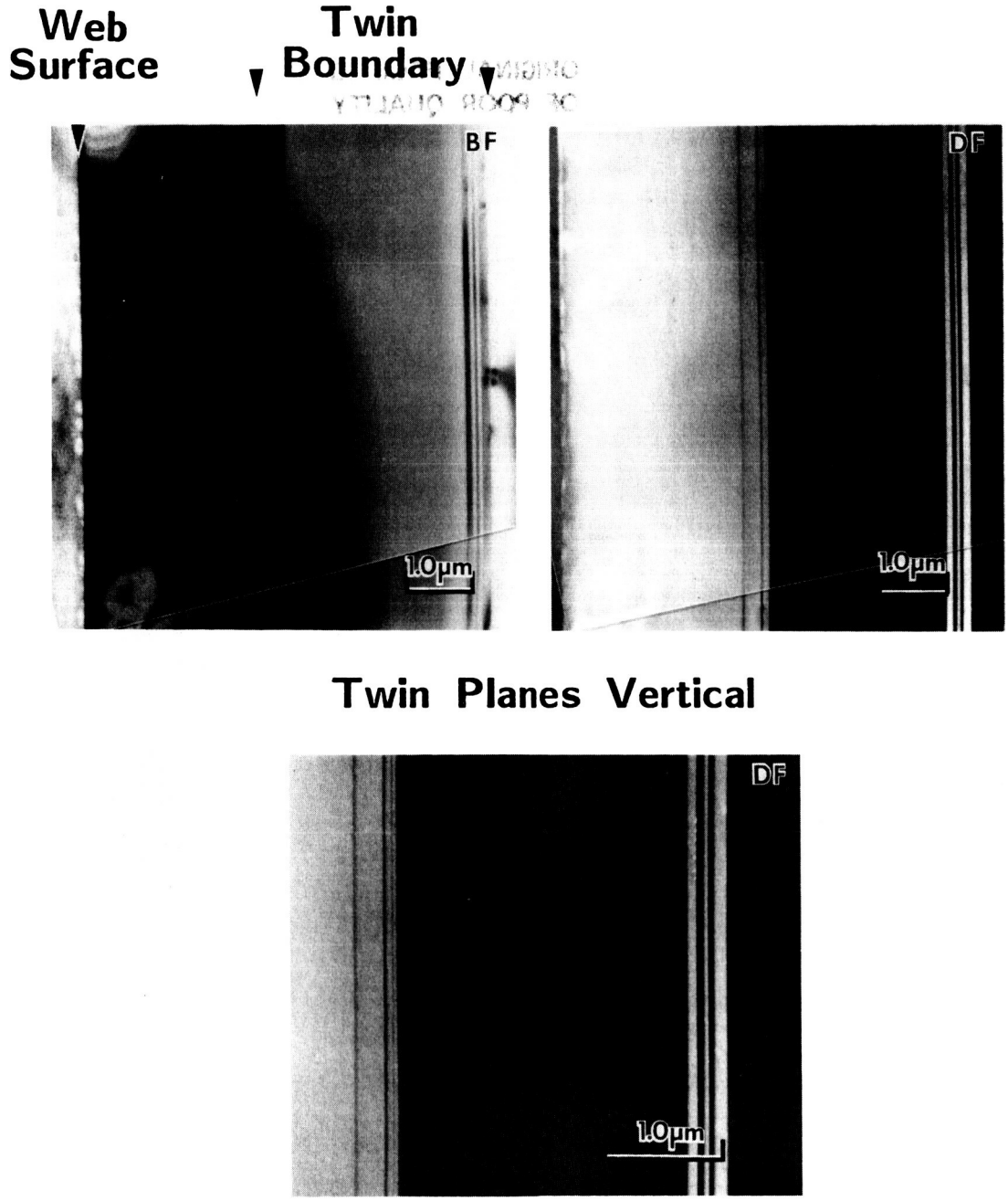

Figure 5 — Cross-sectional TEM view of cell 17B (13%) from section 14 (near the end) of crystal 2-297-16 showing 13 twin boundaries distributed over 3.3 μm in depth and twin boundaries within 2.6 μm of the external surface.

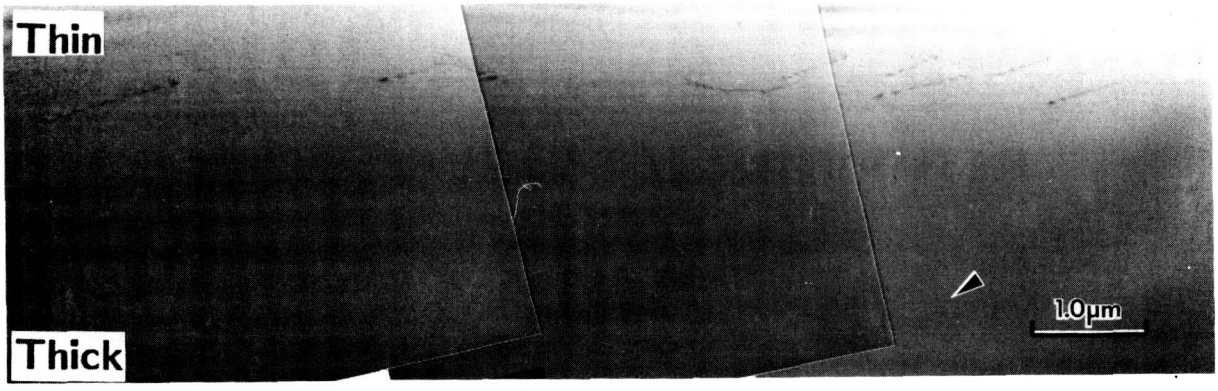

CELL 17B:2297-16.14:(13%)

Twin Planes Tilted

Figure 6 — Cross-sectional TEM view of cell 17B with twin planes tilted showing a dislocation density of 3.6×10^7 dislocations/cm^2 in the heavily twinned region.

CELL 17B:2297-16.14:(13%)

Bulk Web Structure

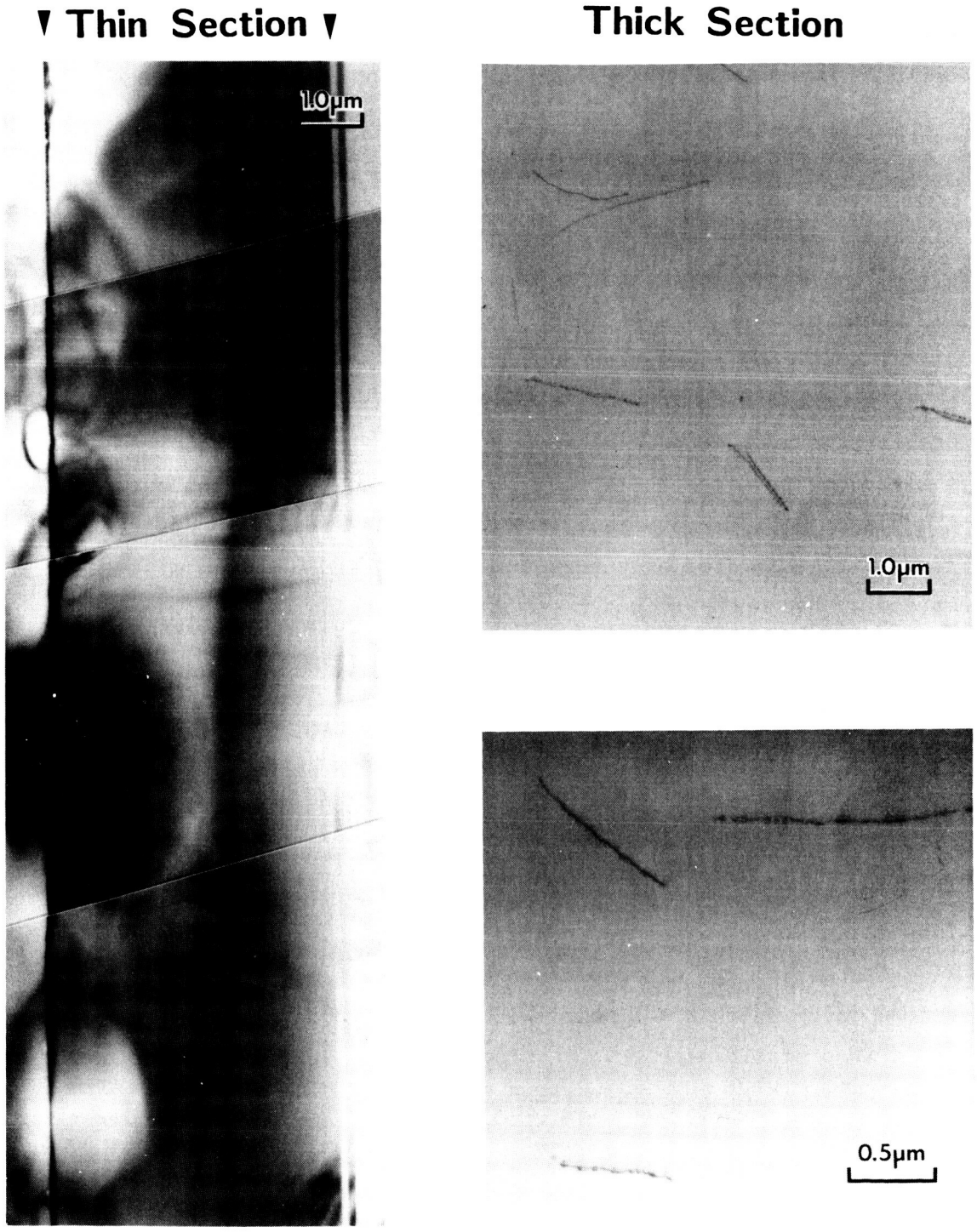

Figure 7 — Cross-sectional TEM view of bulk structure in cell 17B showing no dislocations in the thin section between the external surface and the twin planes, but dislocations present in the thick section on the opposite side of the twin planes.

program, hydrogen ion implantation is being investigated to passivate the dislocation/precipitate defects that have been observed in web cells.

It has not been determined whether the dislocations alone, the precipitates which decorate the dislocations alone, or the dislocation/precipitate combination is responsible for limiting the diffusion length in web cells. However, recent work[2,3] has shown that SiO_x precipitates in silicon do introduce defect levels which are distributed continuously throughout the bandgap. These defect levels arise from the dangling silicon bonds at the interface between the SiO_x precipitate and the bulk silicon. Such levels appear to be quite similar to the interface states that have been studied extensively for the planar SiO_2/Si interface in MOS devices. These interface states are routinely passivated by a heat treatment at 450°C for 15 minutes in a molecular hydrogen ambient.

It may be that the dislocations in web material act as effective nucleation sites for SiO_x precipitates, and that it is the precipitates themselves which limit the diffusion length in web cells. Since web is grown with a quartz crucible, the web contains a high concentration of dissolved oxygen (19 ppma by ASTM F121-80 IR spectroscopy method).[4] The improvement that has been observed for web cells as a result of hydrogen ion implantation may be associated with the passivation of these interface states. This improvement would then be similar to that observed for MOS devices that are heat treated in a hydrogen ambient. Of course, it is also possible that the hydrogen is passivating dangling bonds along the core of the dislocations.

As described in the previous quarterly progress report for this program, web cells which were completed except for an antireflective (AR) coating were improved by the implantation of hydrogen ions into the emitter side of the cell. The improvement was noted both in the cell

efficiency and in the minority carrier diffusion length, as measured by the surface photovoltage (SPV) technique. However, in the Westinghouse processing sequence the AR coating is applied by a dipping process, and the presence of grid lines prevents the formation of a uniform coating. Earlier attempts to implant hydrogen through the AR coating were not successful. It was decided to attempt to implant hydrogen into the emitter side of the web strips after the high-temperature boron and phosphorus diffusion steps were completed, but before the metallization step. This is expected to provide the desired improvement to the base material while not disturbing the step in which the AR coating is applied. In addition, the possibility of junction degradation by metal diffusing into the depletion region as a result of heating from the ion beam is eliminated if metal grid lines are not present.

The hydrogen ion implantation was done at the Westinghouse R&D Center using a Veeco Microetch system which was adapted for low-energy (1500 eV), high-dose (2 mA/cm^2 for 2 minutes) hydrogen ion implantation. A schematic diagram of the system is given in Figure 8, and a photograph of a web cell during implantation is shown in Figure 9. The results of hydrogen ion implantation into small-area and into full-sized web cells are described below.

3.2.1 Fabrication of Small Area (1 cm^2) Web Cells Including Hydrogen Ion Implantation

Results have been obtained for small cells (1 x 1 cm) fabricated from three different web strips. Each web strip was cut into two pieces after boron and phosphorus diffusions. One piece (e.g., 48) was processed into finished cells without hydrogen ion implantation, while the other piece (e.g., 48H) was implanted and then processed to completion. The results are given in Table 1. A significant improvement in diffusion length, short-circuit current, open-circuit voltage, and efficiency has been obtained as a consequence of hydrogen ion implantation for cells from strips 48 and 63. Cell 48-1, which was not implanted,

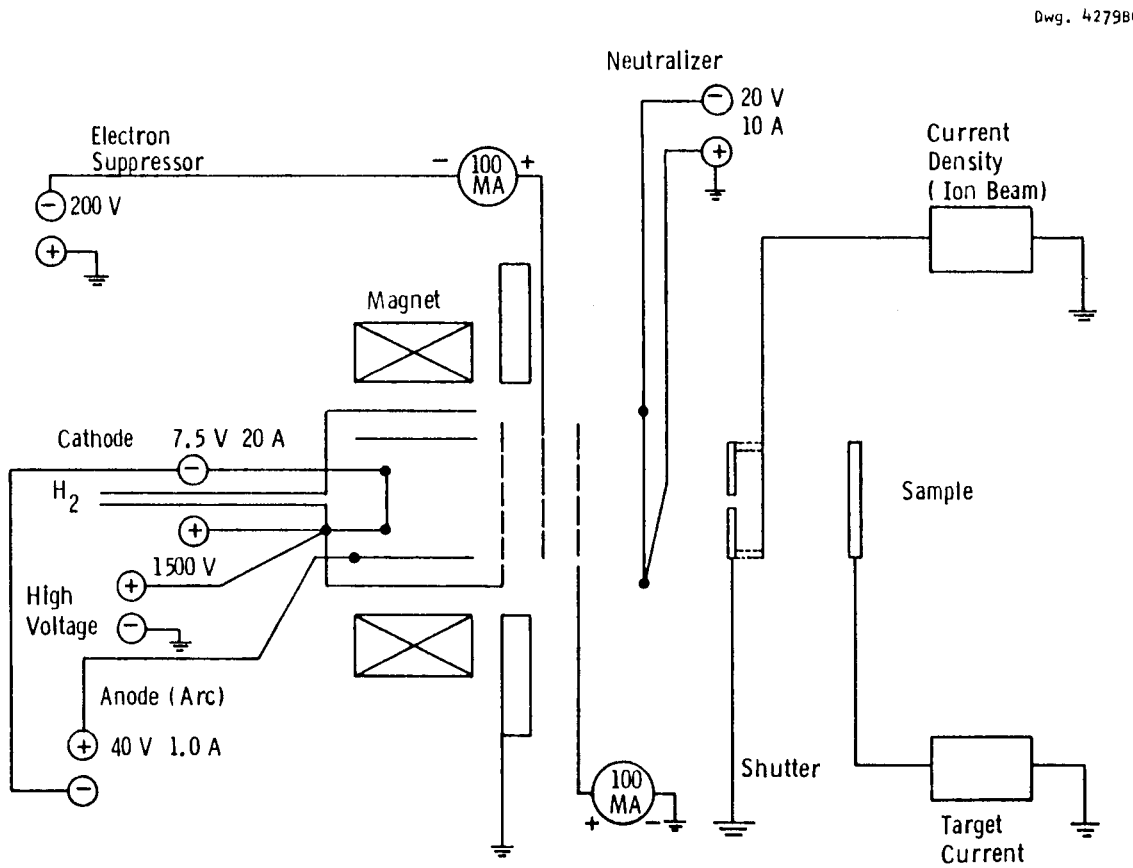

Figure 8 — Schematic diagram of Veeco Microetch system adapted for low-energy, high-dose hydrogen ion implantation.

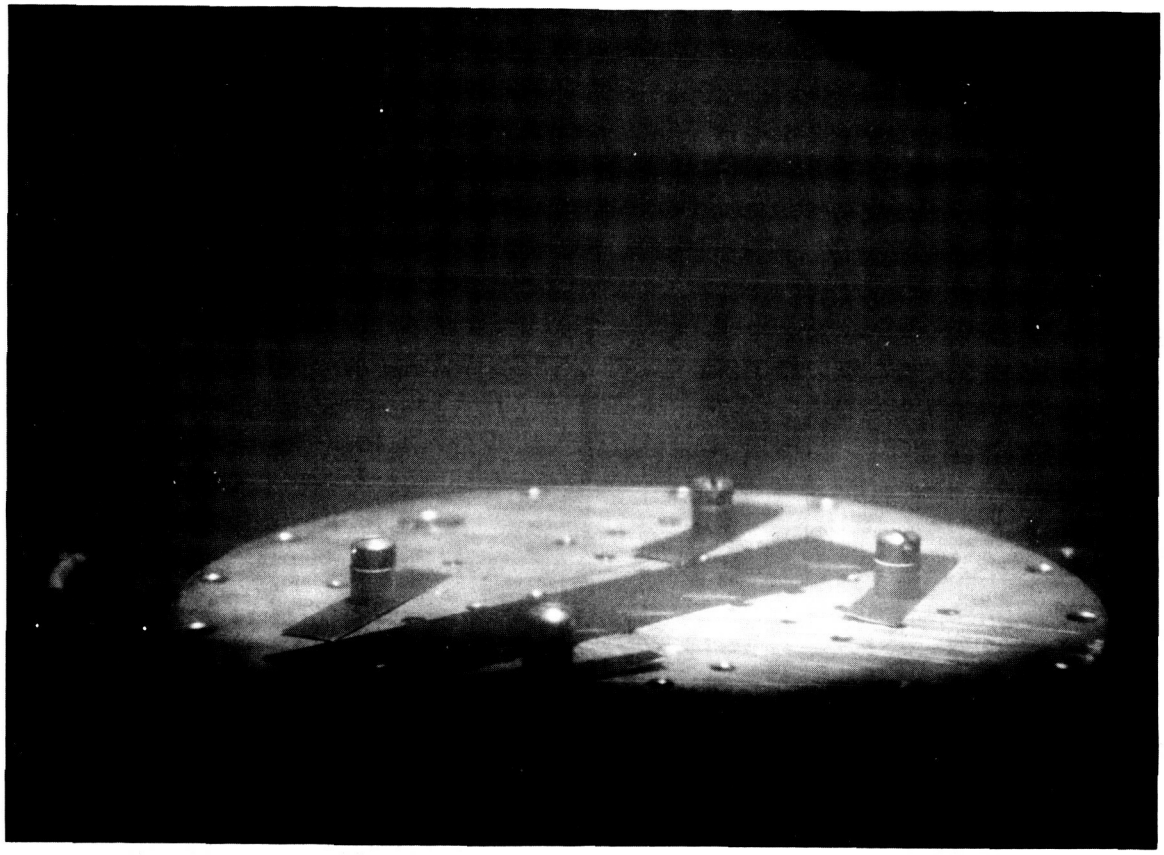

Figure 9 — Photograph of web cell during hydrogen ion implantation (the light for exposing the photographic film came from a violet glow associated with the hydrogen ion beam).

Table 1. Effect of Hydrogen Ion Implantation on Web Cells

A. Before Anti-Reflective Coating

Web Cell ID	Crystal ID	H^+ Implant	J_{sc} (mA/cm^2)	V_{oc} (V)	FF	η (%)	SPV L_n (μm)
48-1	6-311-17.13	No	21.3	0.502	0.748	8.01	19
48H-1	"	Yes	24.1	0.561	0.771	10.4	120
63-2	2-303-13.9	No	22.2	0.521	0.771	8.91	21
63X-2	"	Yes	24.2	0.558	0.753	10.2	160
52-1	4-305-7.8	No	24.7	0.565	0.770	10.8	130
52H-1	"	Yes	24.8	0.572	0.757	10.8	>200

B. After Anti-Reflective Coating (600 A ZnS, 1000 A MgF_2)

Web Cell ID	H^+ Implant	J_{sc} (mA/cm^2)	V_{oc} (V)	FF	η (%)
48-1	No	32.0	0.510	0.729	11.9
48H-1	Yes	36.4	0.574	0.770	16.1
52-1	No	36.8	0.586	0.773	16.7
52H-1	Yes	36.7	0.589	0.757	16.4

Notes:
1. Implant Conditions: 1500 eV, 2 mA/cm^2, 2 minutes with no stage cooling.
2. Hydrogen was implanted into the emitter side of the cells after boron and phosphorus diffusions.
3. Cell size: 1x1 cm.
4. Test Conditions: AM1 (tungsten/halogen lamp), 100 mW/cm^2, room temperature (Run Cell-4).
5. Starting web material was boron-doped to 4 ohm-cm.

had an efficiency of 8.01% (no AR coating) and a diffusion length of 19 μm. Cell 48H-1, which was implanted, had an efficiency of 10.4% and a diffusion length of 120 μm. With a double-layer antireflection coating (600 A ZnS and 1000 A MgF_2) the efficiencies are 11.9% without implantation and 16.1% with implantation. Similar improvements were realized for the cells fabricated from strip 63.

Cell 52-1 had a high efficiency of 10.8% (no AR coating) without implantation. Cell 52H-1, from the same web strip as 52-1, was not affected by the implantation. After the application of the double-layer AR coating, the efficiency exceeded 16% in both cases. These results suggest that hydrogen ion implantation may be quite effective in improving the base material for most web cells, but that cells made from superior quality web may be improved only marginally.

Hydrogen ion implantation into low-resistivity (0.2 ohm-cm) web after boron and phosphorus diffusions is planned for the future. If hydrogen is able to passivate the defect states in the bandgap for this low-resistivity material, it may be possible to realize the benefits of the low resistivity to the open-circuit voltage without sacrificing diffusion length, and consequently short-circuit current. Web material for this experiment is scheduled to be grown, and the effects of hydrogen ion implantation will be investigated for the first time.

3.2.2 Fabrication of Full-Sized Web Cells Including Hydrogen Ion Implantation

Twenty-two web strips, each 33 cm in length, were processed through boron and phosphorus diffusions at the Westinghouse Advanced Energy Systems Division (AESD). After the diffusions, each strip was cut into two pieces, one 22 cm long and the other 11 cm long. The 11 cm pieces were then implanted with hydrogen using the modified Veeco Microetch system with a 4-inch ion beam at the Westinghouse R&D Center. The implant conditions included a beam energy of 1500 eV, a beam current

density of 2.0 mA/cm^2 (as measured by a Faraday cup), and an implant time of 2.0 minutes. No external heating of the sample stage was used, and two 11 cm long strips were implanted at the same time.

The 22 web strips (11 cm long) that had been implanted with hydrogen after boron and phosphorus diffusions were returned to AESD, where full-sized cells (2.9 x 9.8 cm) were fabricated from the implanted strips using the standard processing sequence. These cells were then compared with cells fabricated at the same time and from the same web crystal section, but without a hydrogen implant. The results are given in Table 2 and in Figures 10 and 11.

Measurements of the minority carrier diffusion length (SPV) and lifetime (OCD) indicated an improvement of the bulk material for most of the implanted cells. It was found that a significant improvement (1.2 to 1.9 mA/cm^2) in J_{sc} was obtained for cells with J_{sc} < 30 mA/cm^2, but that for cells with J_{sc} above this value there was no systematic change. The largest improvement was for cells from strip 35, for which J_{sc} increased from 29.1 to 31.0 mA/cm^2 as a result of hydrogen implantation. The minority carrier diffusion length and lifetime increased from 14 to 56 μm and from 3.5 to 6.9 μs, respectively, for these cells.

Some cells exhibited a significant decrease in fill factor following hydrogen ion implantation because of a large series resistance (2.3 to 7.8 ohm-cm^2). This may be associated with implant damage which could render the first few hundred angstroms of silicon amorphous, or with an etching of the emitter surface by the hydrogen ion beam.

An additional batch of web strips (11 cm long) which have undergone both diffusions has been supplied by AESD. The above experiment will be repeated after measurements of beam uniformity and sample temperature during implantation have been made. In addition, measurements of cross-sectional TEM and EBIC are scheduled for four samples in

Table 2 — Comparison of Full-Sized Cells with and without Hydrogen Ion Implantation

Sample ID	Pair	Crystal	J_{sc} (mA/cm^2)	V_{oc} (V)	FF	η (%)	SPV L_n (μm)	τ_{ocd} (μs)
20A	1	2-245-8.13	29.7	0.551	0.760	12.4	12	3.9
21H	1	2-245-8.14	31.0	0.563	0.731	12.8	58	4.7
23A	2	2-245-8.16	31.1	0.579	0.727	13.1	59	8.7
23H	2	"	30.6	0.567	0.777	13.5	92	8.0
34AX	3	J-557-2.4	31.9	0.579	0.755	14.0	146	17.5
34H	3	"	32.0	0.575	0.773	14.2	154	18.2
35AX	4	-	29.1	0.532	0.714	11.1	12	3.5
35H	4	-	31.0	0.554	0.659	11.3	67	6.9
39AX	5	J-558-2.5	30.0	0.568	0.755	12.9	30	5.1
39H	5	"	31.2	0.567	0.765	13.5	80	9.8
41AX	6	N-128-16.4	31.6	0.576	0.791	14.4	40	6.8
41H	6	"	31.1	0.564	0.714	12.5	133	7.7
43A	7	N-132-4.4	31.8	0.559	0.801	14.2	41	12.5
43H	7	"	24.0	0.553	0.304	4.0	62	11.1
47A	8	7-294-12.8	30.2	0.558	0.759	12.8	24	6.0
47H	8	"	29.1	0.566	0.581	9.6	110	11.5
48AX	9	7-294-12.13	31.0	0.563	0.766	13.4	41	8.6
48H	9	"	28.7	0.561	0.464	7.5	120	15.5

Note:

Cell size is 2.9 x 9.8 cm. The implanted samples from pairs 7, 8, and 9 had excessive series resistance (2.3-7.8 ohm-cm^2). Suffix "H" in Sample ID identifies cell which had been implanted in pair.

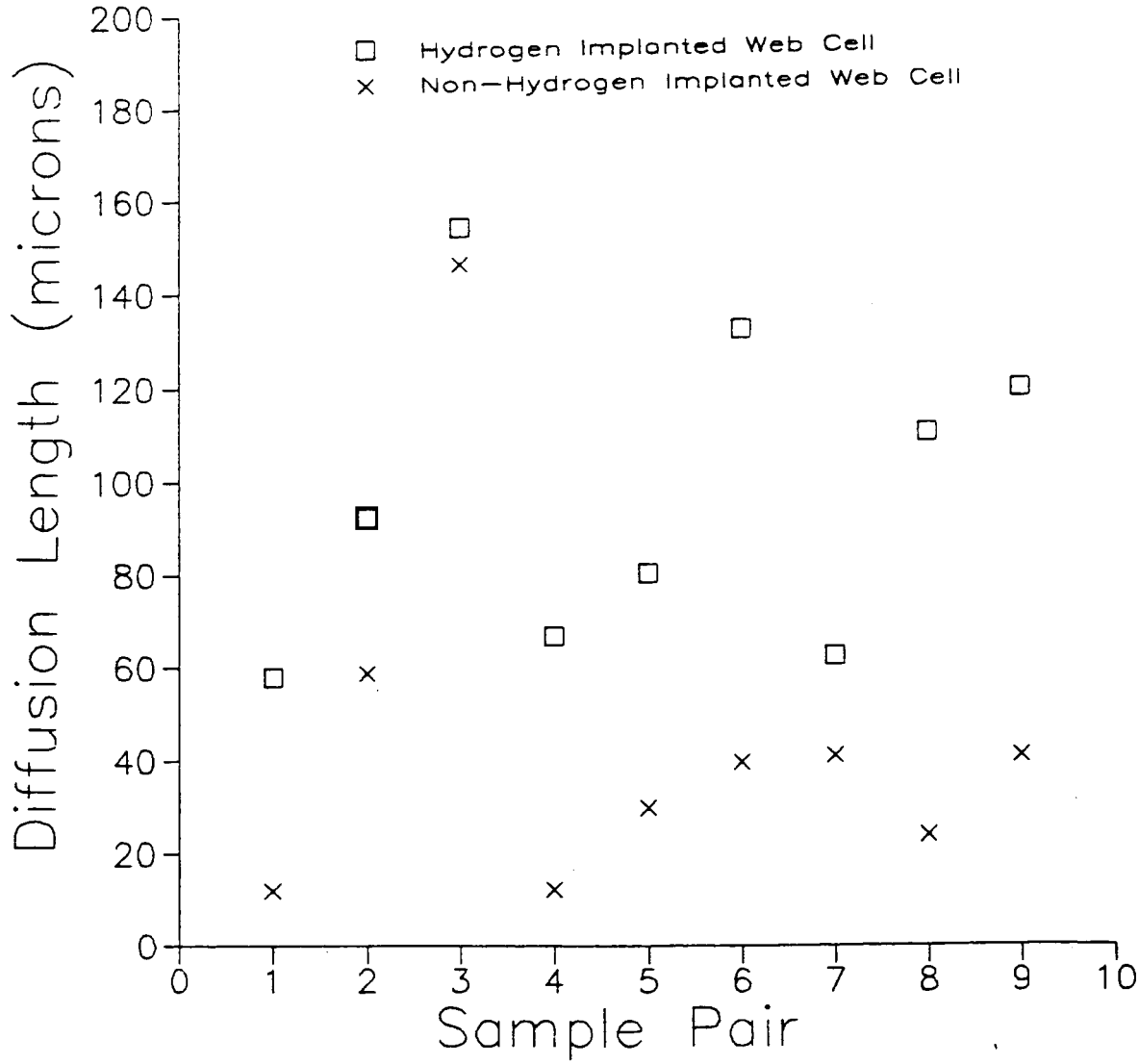

Figure 10 — Effect of hydrogen ion implantation on electron diffusion length in full-sized (28.4 cm^2) web cells.

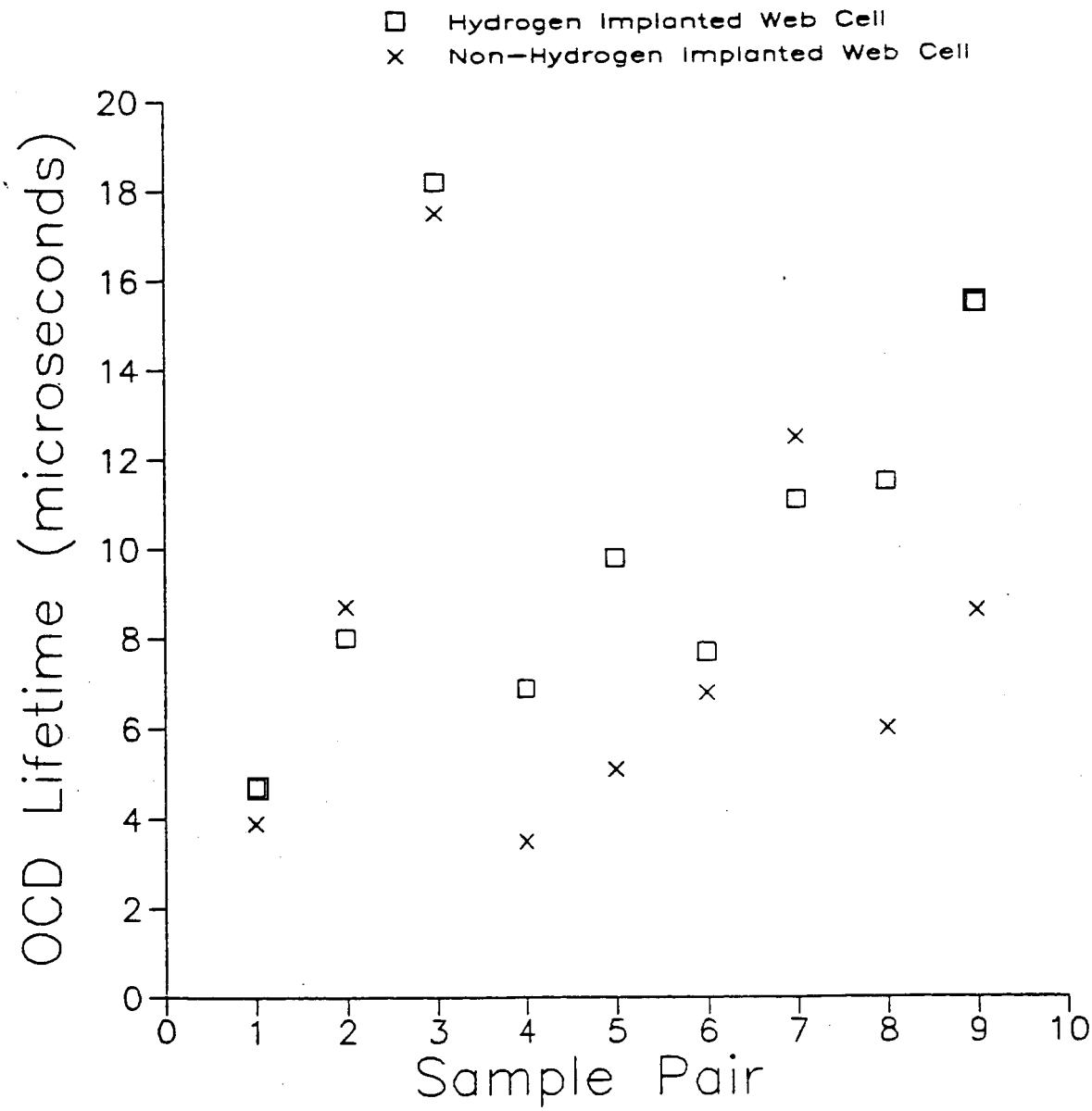

Figure 11 — Effect of hydrogen ion implantation on electron lifetime in full-sized (28.4 cm^2) web cells.

an attempt to clarify which defects are being passivated by the hydrogen.

3.3 FABRICATION OF WEB AND FLOAT ZONE SILICON CELLS

Cells that are 2 x 2 cm in size, as required by the contract, have been fabricated from web silicon substrates and float zone silicon substrates. Examples of such cells are shown in Figure 12. Both substrates are boron-doped. The web substrate has a nominal resistivity of 4 ohm-cm with a (111) surface and the Wacker float zone substrate has a resistivity of 0.2 ohm-cm with a (100) surface. The cell area is defined by a mesa etch. The nominal thickness is 130 μm for the web cells and 375 μm for the float zone cells.

3.3.1 Process Sequence and Cell Efficiencies

The process sequence for fabricating the cells is summarized in Figure 13. The emitter region is formed by a $POCl_3$ diffusion at 850°C and the back surface field region is formed by a BBr_3 diffusion at 950°C. The samples are cooled slowly (1°C/min) to 600°C after each diffusion. Both front and back surfaces are passivated with a thin (100 A) SiO_2 layer grown at 800°C. Again, the samples are cooled slowly to 600°C after the oxide passivation step. Contact is made to the silicon in a grid line pattern on the front and back of the cell. An aluminum back surface reflector (1000 A) is deposited over the entire back surface. After the evaporated metal layers are plated with 8 μm of silver, a double-layer antireflective coating is deposited on the front of the cell by evaporation. This coating consists of 430 A of ZnS deposited on the SiO_2, and 1000 A of MgF_2 deposited on the ZnS. These thicknesses are optimum values for a silicon surface with a layer of SiO_2 100 A thick.

The results for eight web cells and two float zone cells are given in Table 3. The best web cell had an efficiency of 16.5%, and the best float zone cell had an efficiency of 18.3%. The eight web cells

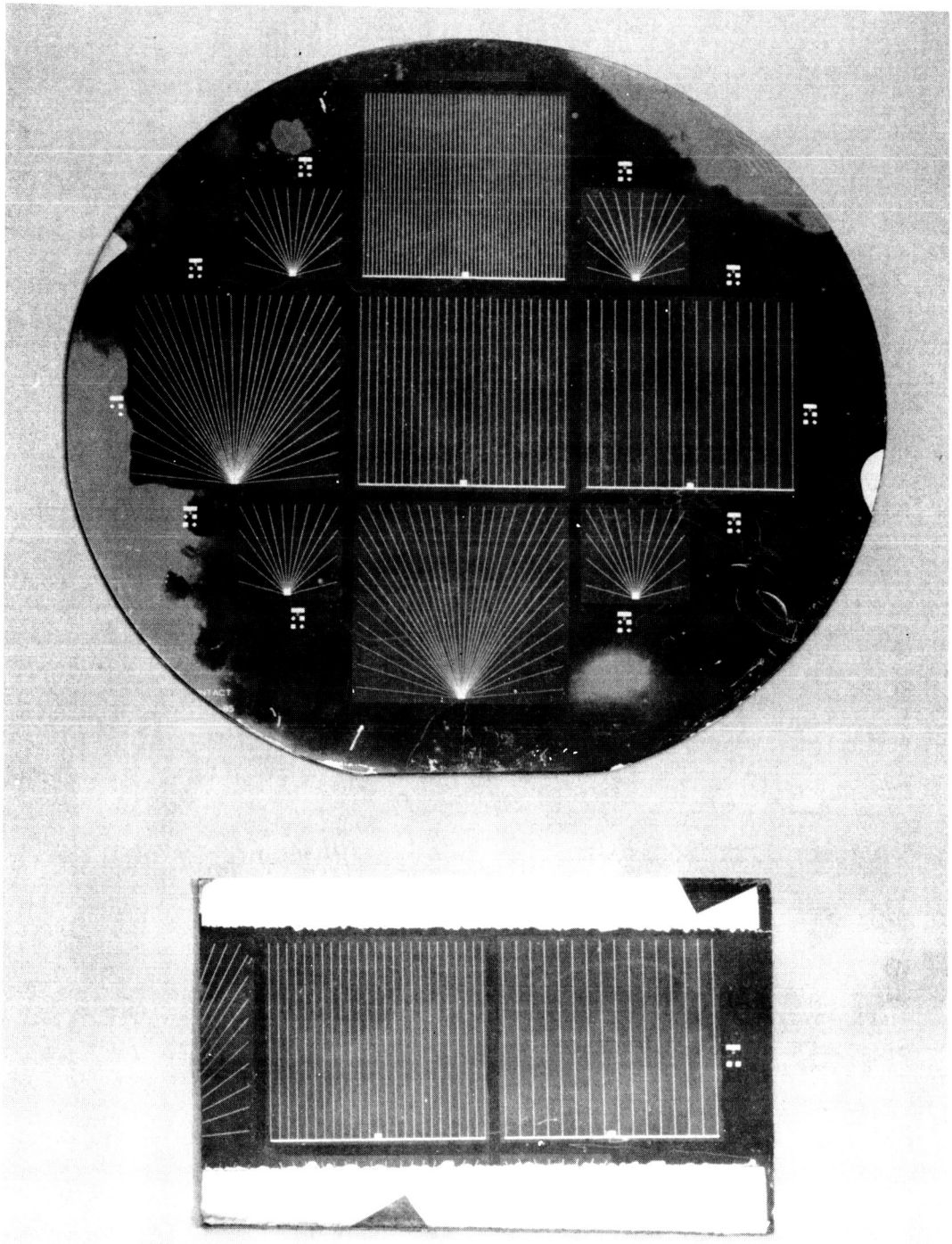

Figure 12 — Photograph of solar cells fabricated with a dendritic web silicon substrate (nominal 4 ohm-cm) and with a float zone silicon substrate (nominal 0.2 ohm-cm). Substrates are boron-doped, and cell size is 2x2 cm for the seven larger cells shown.

Dwg. 4279B09

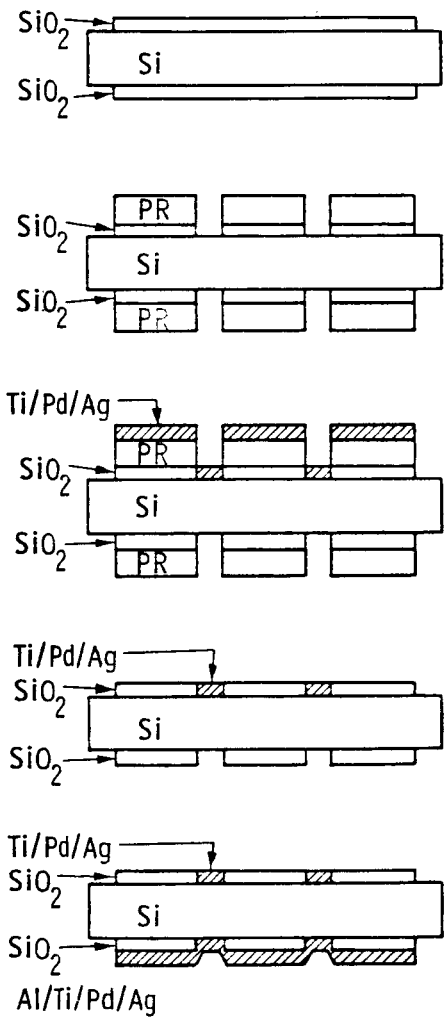

1. Oxide-Passivation Layers on Diffused Silicon

2. Grid Line Contact Windows Etched in Oxide Front and Back.

3. Front Metal Evaporation (Ti/Pd/Ag)

4. Metal Rejection; Front Grid Lines Contact Silicon

5. Back Metal Evaporation (Al/Ti/Pd/Ag) ; Back Grid Lines Contact Silicon

Figure 13 — Process sequence for metal contact to silicon along grid line openings in oxide.

Table 3 — Cells Produced by the High-Efficiency Process (Run Cell-3)

Cell ID	Substrate	J_{sc} (mA/cm^2)	V_{oc} (V)	FF	η (%)	QE L_n (μm)	τ_{ocd} (μs)	Thickness (μm)
A-1	web	36.6	0.573	0.772	16.2	----	----	124
A-2	web	37.1	0.571	0.765	16.2	149	16	124
C-1	web	34.2	0.583	0.773	15.4	----	----	127
C-2	web	36.0	0.584	0.769	16.2	62	11	127
E-1	web	36.5	0.577	0.766	16.1	----	----	140
E-2	web	37.5	0.576	0.762	16.5	116	38	140
11M-1	web	34.7	0.579	0.750	15.1	----	----	122
11M-2	web	35.0	0.579	0.741	15.0	59	10	122
3FZH-5	float zone	36.3	0.625	0.804	18.2	----	----	394
3FZH-7	float zone	35.9	0.626	0.812	18.3	210	18	394

Notes:

1. Cell Size: 2 x 2 cm
2. Test Conditions: AM1 (tungsten/halogen lamp), 100 mW/cm^2 room temperature.
3. Web substrates were boron-doped to 4 ohm-cm (nominal); float zone substrates were boron-doped to 0.2 ohm-cm (Wacker 100)
4. Surface Passivation: 100 Å SiO_2 (front and back).
5. Antireflective coating: 430 Å ZnS and 1000 Å MgF_2 (evaporated)
6. Back surface reflector: 1000 Å Aluminum.
7. 11M cells were produced by a modified process with dot contacts through the oxide (front and back).
8. Forward current for τ_{ocd} measurement: 150 mA (~ I_{sc})

listed in Table 3 were shipped to JPL as deliverables under this contract.

It is interesting to note that J_{sc} for the best web cell (37.5 mA/cm^2) exceeded that for the best float zone cell (35.9 mA/cm^2). This is supported by a higher value for the electron lifetime in the base of the web cell (38 μs) as compared with the lifetime value for the float zone cell (18 μs). The lifetimes were measured by the open-circuit voltage decay (OCD) technique with a forward current of 150 mA (37.5 mA/cm^2). In order to approximate the conditions of the cell under one sun illumination, the magnitude of this forward current was chosen to match the short-circuit current of the cell. At this value of forward current, the base of the cell is under the condition of low-level minority carrier injection.

If these lifetimes are converted into equivalent diffusion lengths ($L_n = [D_n \tau_n]^{1/2}$), the corresponding values are 350 μm for web cell E-2 and 180 μm for float zone cell 3FZH-7. These values of diffusion length are consistent with those required to obtain the magnitude of short-circuit current that was observed. Calculations using the program SPCOLAY were described in the previous quarterly report for this program. These calculations relate the short-circuit current to be expected from a silicon cell 150 μm thick for various values of diffusion length. With a diffusion length of 300 μm, the expected current is 37.0 mA/cm^2 (assuming 5% shadowing and reflection losses). With a diffusion length of 150 μm, the expected current is 35.6 mA/cm^2. These calculated currents agree quite well with the currents observed in the two cells, in which the diffusion lengths extracted from the OCD measurements were 350 μm and 180 μm, respectively.

Also given in Table 3 are values of electron diffusion length in the base as determined from Quantum Efficiency measurements (QE L_n).

These measurements are made under very low-level injection conditions (0.001 sun). For this reason, the diffusion length is expected to be less than the diffusion length under one sun illumination, where some fraction of the traps are saturated, and thereby rendered inactive. In addition, if the true value of the diffusion length exceeds the cell thickness, then the measured value will be limited to approximately the thickness of the cell. Thus, the value of diffusion length obtained from Quantum Efficiency measurements is thought to be a useful indicator of the electrical quality of the base material, but a more accurate value of diffusion length at one sun intensity is taken to be the value derived from OCD measurements.

Contact is made to the silicon in a grid line pattern on both the front and back of the cell. In the case of all cells in Table 3 except 11M-1 and 11M-2, windows are etched in the passivating oxide so that metal touches silicon along the full length of the line ("high-efficiency" process). In the case of cells 11M-1 and 11M-2, 20 μm square windows having an 800 μm spacing are etched in the oxide ("modified high-efficiency" process). This reduces the area of metal in direct contact with the silicon by a factor of 40 compared to the full grid line contact, and thereby significantly reduces the recombination activity associated with the metal/silicon interface.

To date, the dot contact metallization pattern has not produced an improvement in cell performance in either web cells (4 ohm-cm base) or in float zone cells (0.2 ohm-cm base). The contact area is adequate, since the fill factor of cells produced in this way is in the normal range. The lack of improvement indicates that the carrier recombination in the emitter may not be dominated by the metal contacts. It could, for example, be dominated by the heavily doped region very near the surface of the emitter. An effort has been initiated to address this effect by creating the emitter region with an arsenic source rather than a phosphorus source. This would permit a reduction in the surface

concentration of the emitter from 1 x 10^{20} cm^{-3} to 1 x 10^{19} cm^{-3}, and is expected to reduce the recombination activity in the emitter.

3.3.2 ZnS/MgF_2 Double-Layer Antireflective Coating

During this reporting period the ZnS/MgF_2 double-layer AR coating was optimized for a silicon substrate with a passivating oxide layer 100 A thick. The index of refraction, as determined from ellipsometry measurements, is 2.35 for ZnS and 1.38 for MgF_2. In the last quarterly progress report for this program, a choice of 600 A ZnS and 1000 A MgF_2 was shown to be very effective when deposited on bare silicon. An enhancement in J_{sc} of 50% was obtained experimentally relative to the J_{sc} value for bare silicon. The choice of thicknesses for the case with oxide passivation was guided by calculations. In Figure 14, curves of constant improvement in short-circuit current are given as a function of layer thickness for layers with an index of refraction of 2.4 and 1.4. These indices are reasonably close to those measured for ZnS (2.35) and MgF_2 (1.38), respectively.

With the thickness of MgF_2 held at a constant value of 1000 A, thicknesses of 380, 430, 450, 500, and 540 A of ZnS were deposited. The best value was found to be 430 A, in reasonable agreement with the calculated values of Figure 14. The measured reflectivity of cell E-2 from Table 3 is given in Figure 15. Note that the reflectivity is less than 5% from 0.4 μm to nearly 1.0 μm. The higher reflected intensity at the longer wavelengths is at least partly attributed to the reflection of the light from the aluminum at the back of the cell. The thicknesses that were deposited on cell E-2 were 430 A for ZnS and 1000 A for MgF_2.

The deposition of these layers is by evaporation. The crystals of ZnS or MgF_2 are placed in a tantalum boat 5 mils thick. In the case of ZnS, a platinum mesh is spot-welded to cover the boat to prevent the crystals from being thrust out of the boat when the material is heated

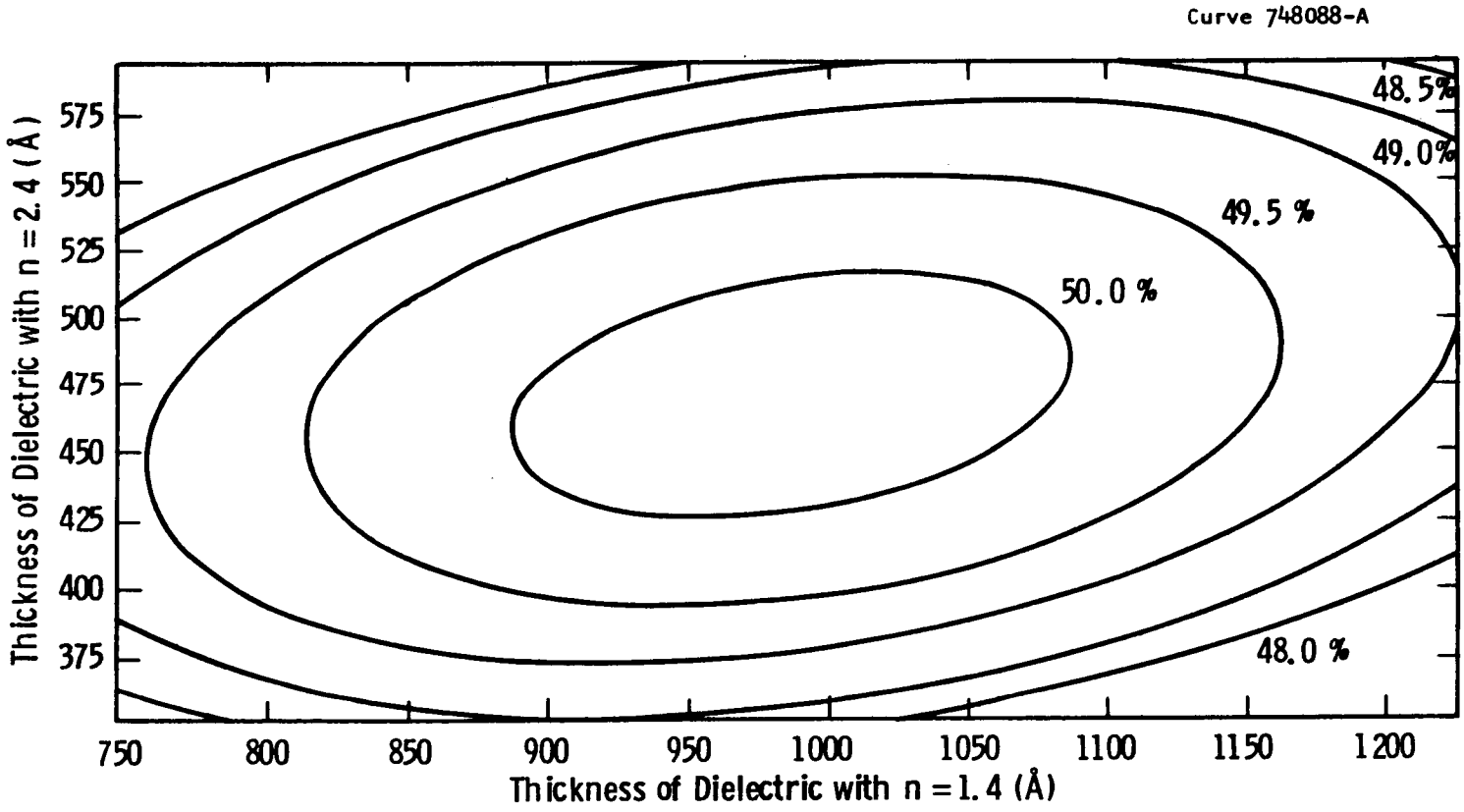

Figure 14 — Calculated improvement in short-circuit current relative to bare silicon for a double-layer antireflective coating deposited on top of 100 Å passivating oxide on silicon solar cells. The contours of equal performance are shown assuming the index of refraction (n) is 2.4 for the lower layer and 1.4 for the upper layer.

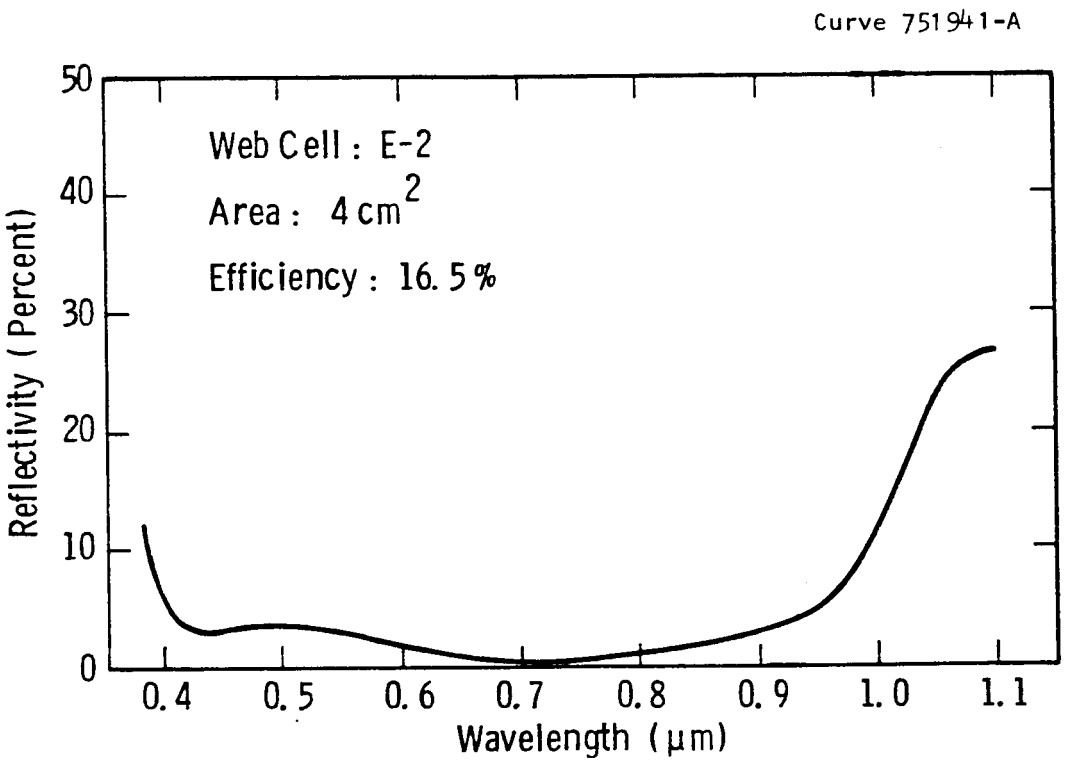

Figure 15 — Reflectivity versus wavelength for web cell E-2 from Run Cell-3. Cell has double-layer antireflective coating (430 Å ZnS and 1000 Å MgF_2) evaporated onto a passivated (100 Å SiO_2) silicon surface.

and sublimes. For ZnS, a current of 90 A is passed through the boat to cause evaporation by resistive heating at a rate of 7 to 11 A/second. For MgF_2, 77 A of current are used to obtain an evaporation rate of 7 to 10 A/second.

3.3.3 Quantum Efficiency Data

The quantum efficiency was measured for the cells indicated in Table 3. Figure 16 shows the measured values for web cell E-2 which had the highest efficiency. Note that the quantum efficiency at 0.4 μm (the minimum wavelength for this measurement) is 80%. This value is quite high, indicating a relatively small amount of recombination occurring in the emitter and at the front surface of the cell. This suggests the oxide passivation is effective in reducing surface recombination. It also suggests that the drift field associated with the variation in doping density in the emitter may be assisting in the collection of holes from the emitter in a significant way. This will be discussed in greater detail in Section 3.3.5.

The plot which is used to obtain electron diffusion length from the quantum efficiency data for web cell E-2 is shown in Figure 17. The reciprocal of the absorption coefficient (α) is plotted against a composite variable (X - 1), and the slope of the straight line gives the diffusion length. The variable "X" is the ratio of the number of photons absorbed in the base of the cell to the number of electrons collected by the emitter-base junction. For this cell, the diffusion length (116 μm) approaches the thickness of the cell (140 μm).

Similar plots of the quantum efficiency data for cells A-2, C-2, and 11M-2 are given in Figures 18, 19, and 20. In all cases the quantum efficiency at 0.4 μm is approximately 80%. This high response at the shorter wavelengths is partly responsible for the large values of short-circuit current that are listed in Table 3. Also contributing to the large current for the web cells is the aluminum back-surface reflector. This reflector is more effective for the thin web cells (130 μm) than

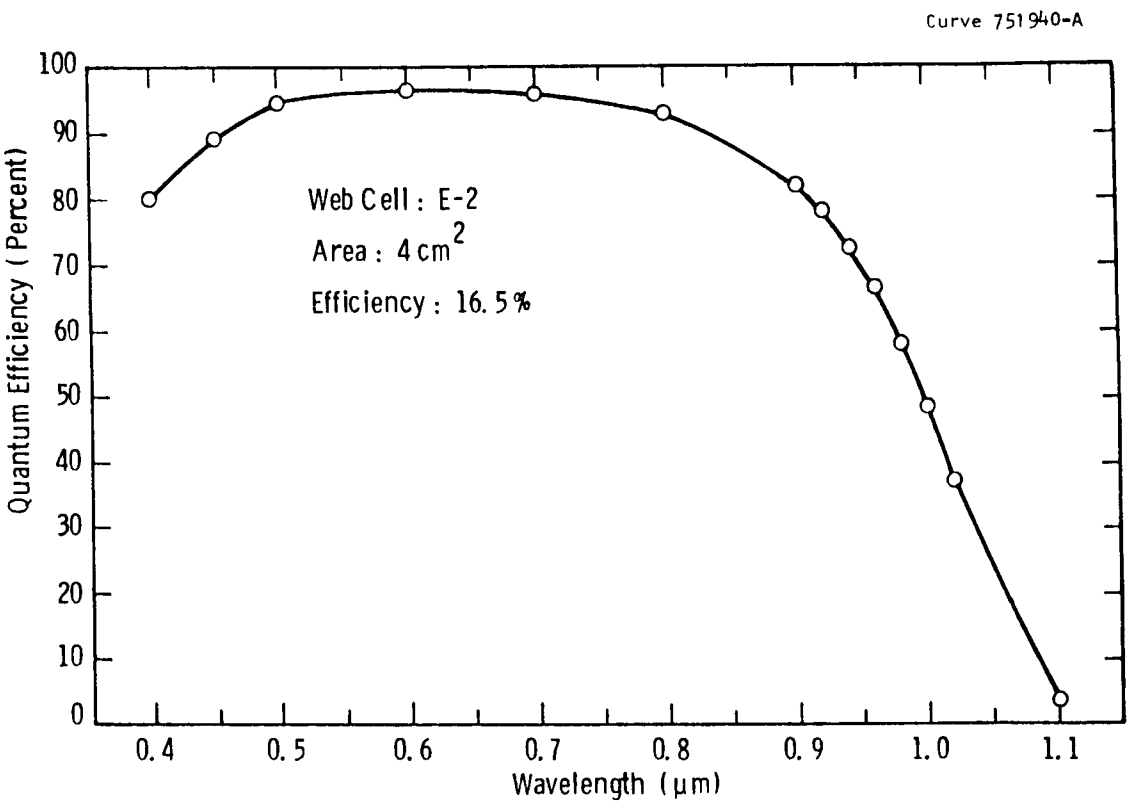

Figure 16 — Quantum efficiency versus wavelength for web cell E-2 from Run Cell-3. Cell has surface passivation (100 A SiO_2), double-layer antireflective coating (430 A ZnS and 1000 A MgF_2), and aluminum back-surface reflector. Web substrate is boron-doped to 4 ohm-cm and efficiency is 16.5%. Note high short-wavelength response.

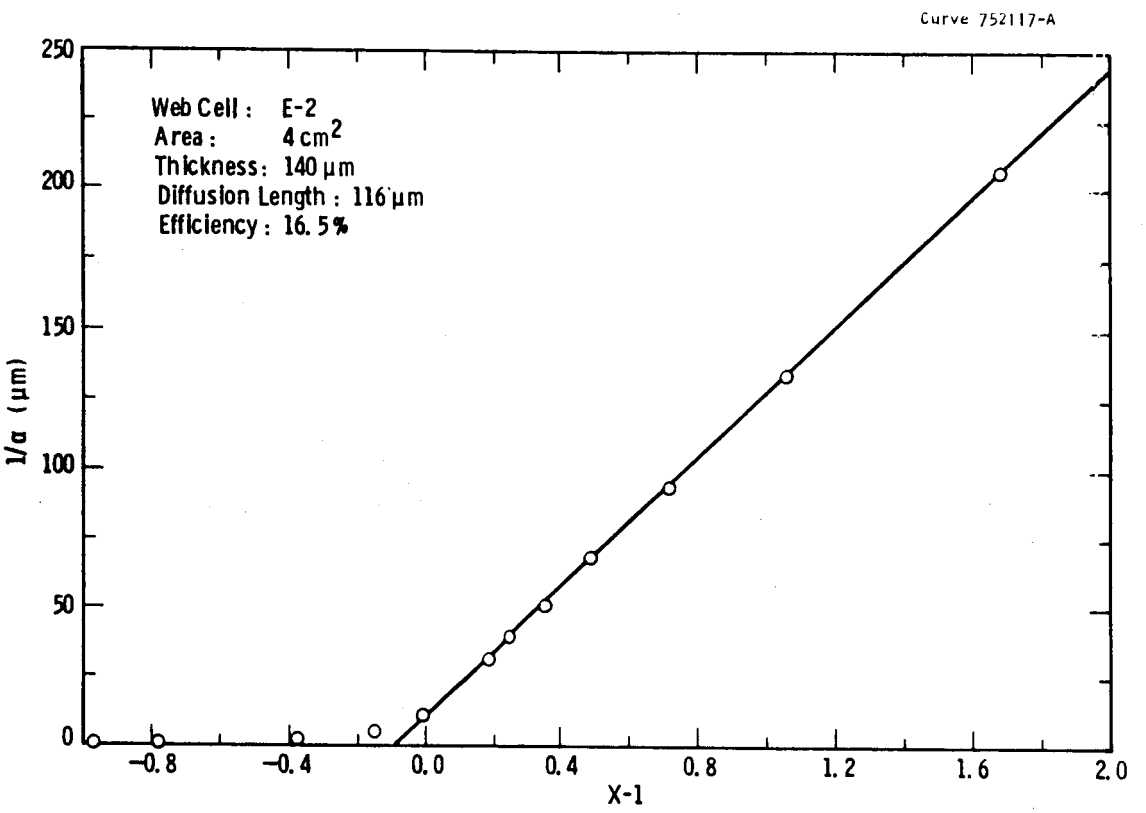

Figure 17 — Plot to determine electron diffusion length for web cell E-2 from Run Cell-3. Note that diffusion length approaches cell thickness.

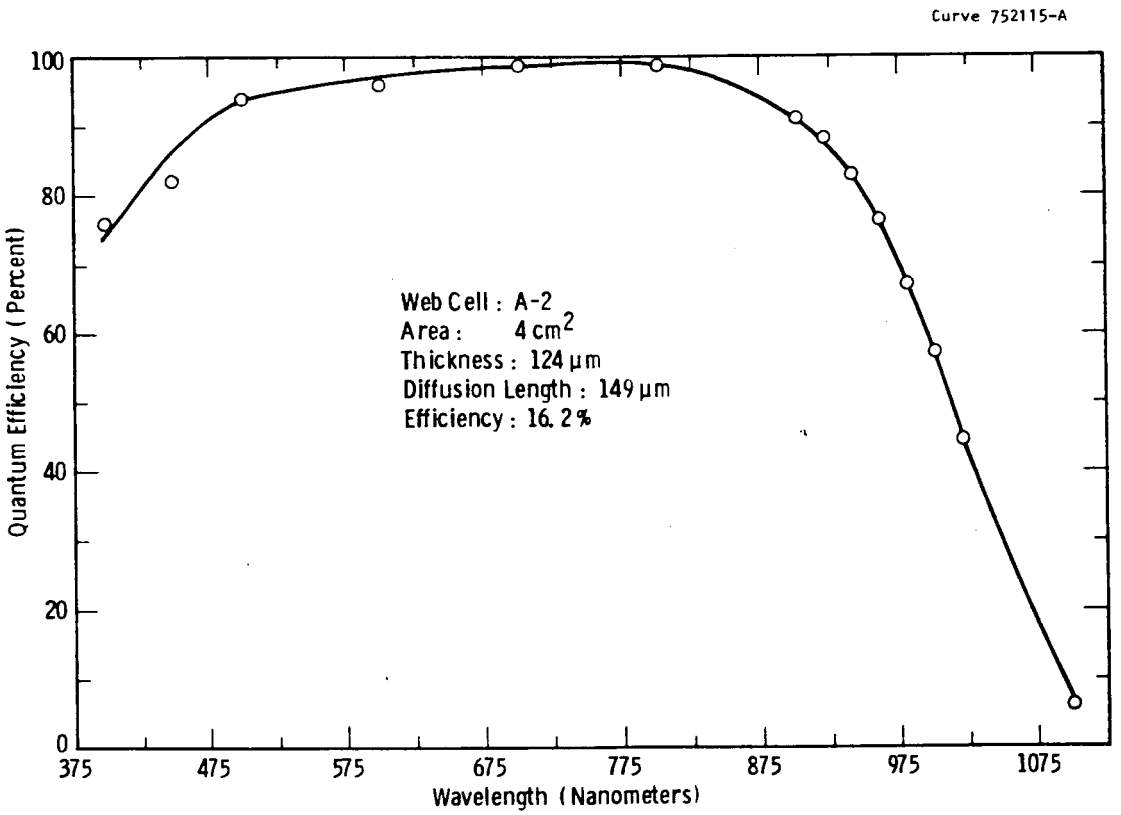

Figure 18 — Quantum efficiency versus wavelength for web cell A-2 from Run Cell-3.

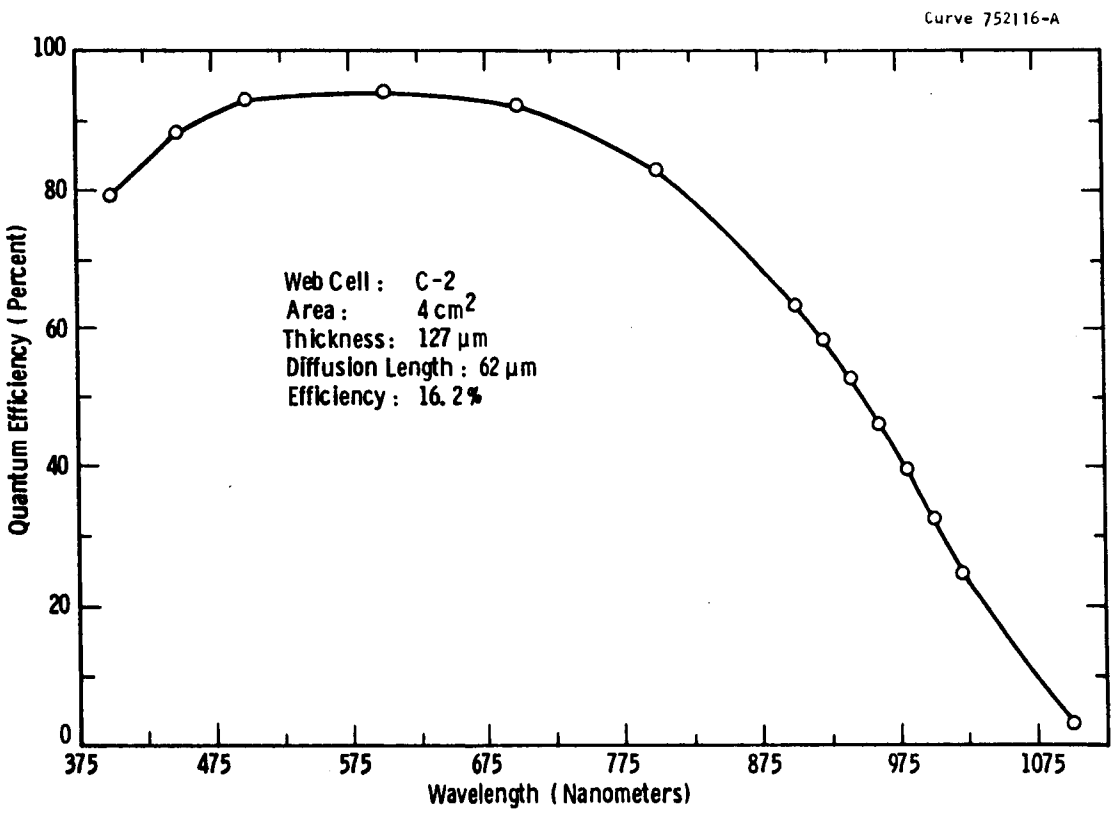

Figure 19 — Quantum efficiency versus wavelength for web cell C-2 from Run Cell-3.

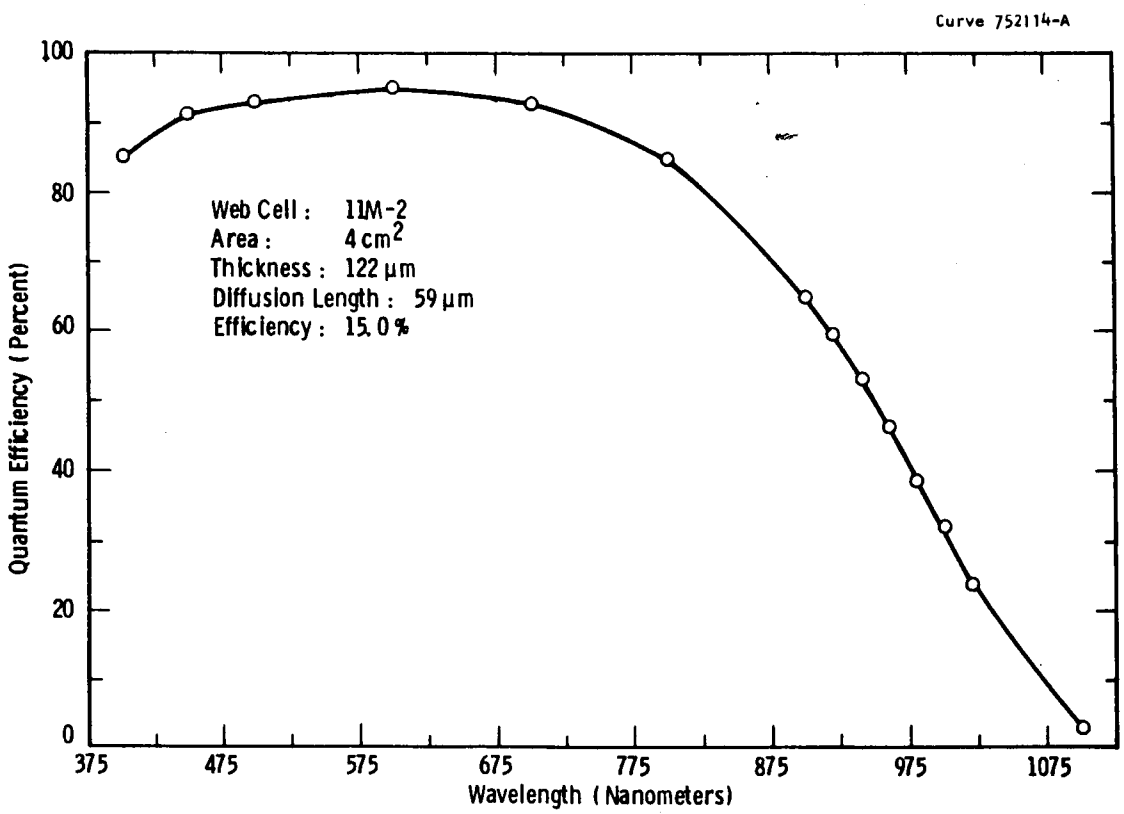

Figure 20 — Quantum efficiency versus wavelength for web cell 11M-2 from Run Cell-3.

for the thicker float zone cells (375 μm) because more of the light is reflected from the aluminum, and the reflected light is then absorbed closer to the collecting junction. Also contributing to the high values of short-circuit current, of course, is the very low loss of light from reflection, as indicated in Figure 15.

3.3.4 Minority Carrier Lifetime by the Open-Circuit Voltage Decay Technique

The values of minority carrier lifetime given in Table 3 were obtained by the open-circuit voltage decay (OCD) technique[5,6] using a Model OCD-2 Lifetime Test Unit from Solid State Measurements, 110 Technology Drive, Pittsburgh, PA 15275. As mentioned above, the forward current was chosen to match the short-circuit current to simulate the conditions under one sun illumination. A photograph of the oscilloscope trace observed in such a measurement is given in Figure 21 for web cell E-2. The voltage falls off linearly with time after the forward bias is removed from the cell. The slope of this line is inversely proportional to the minority carrier lifetime in the base. With $I_{forward} = I_{sc}$, low-level injection conditions apply.

3.3.5 Dopant Profiles and the Drift Field

The dopant profiles for the front (n^+p) and the back (p^+p) junctions for web cell 18M-2 are given in Figures 22 and 23, respectively. Although cell 18M-2 is not listed in Table 3, it was processed in Run Cell-3 and is thus expected to be representative of the cells listed in Table 3. There is an interesting feature to the emitter dopant profile of Figure 22. Since the doping concentration follows a straight line in the semilog plot, the concentration decreases exponentially with depth. The expression describing this decrease is:

$$N_d(x) = N_{do} \exp(-10.7\ \mu m^{-1}\ x). \qquad (1)$$

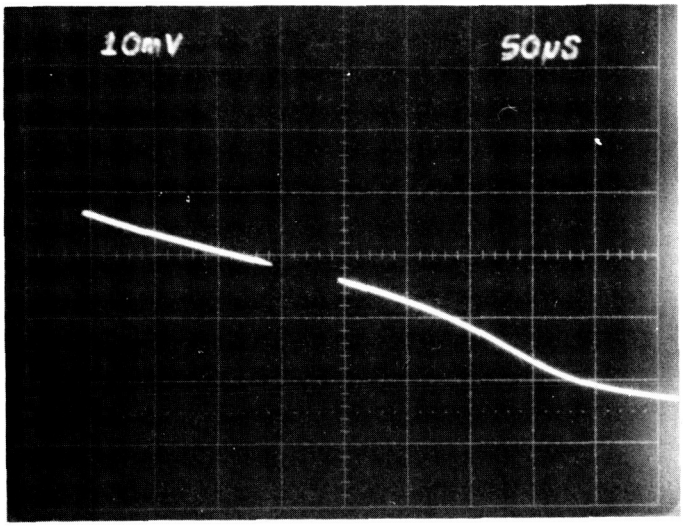

Figure 21 — Oscilloscope trace of the decay of the open-circuit voltage for web cell E-2 of Run Cell-3. The forward current injected into the base was chosen to be 150 mA in order to match the short-circuit current under illumination. The gap in the curve marks the time at which the measurement was made. The lifetime of electrons in the p-type base (τ_{ocd}) was determined to be 38 μs.

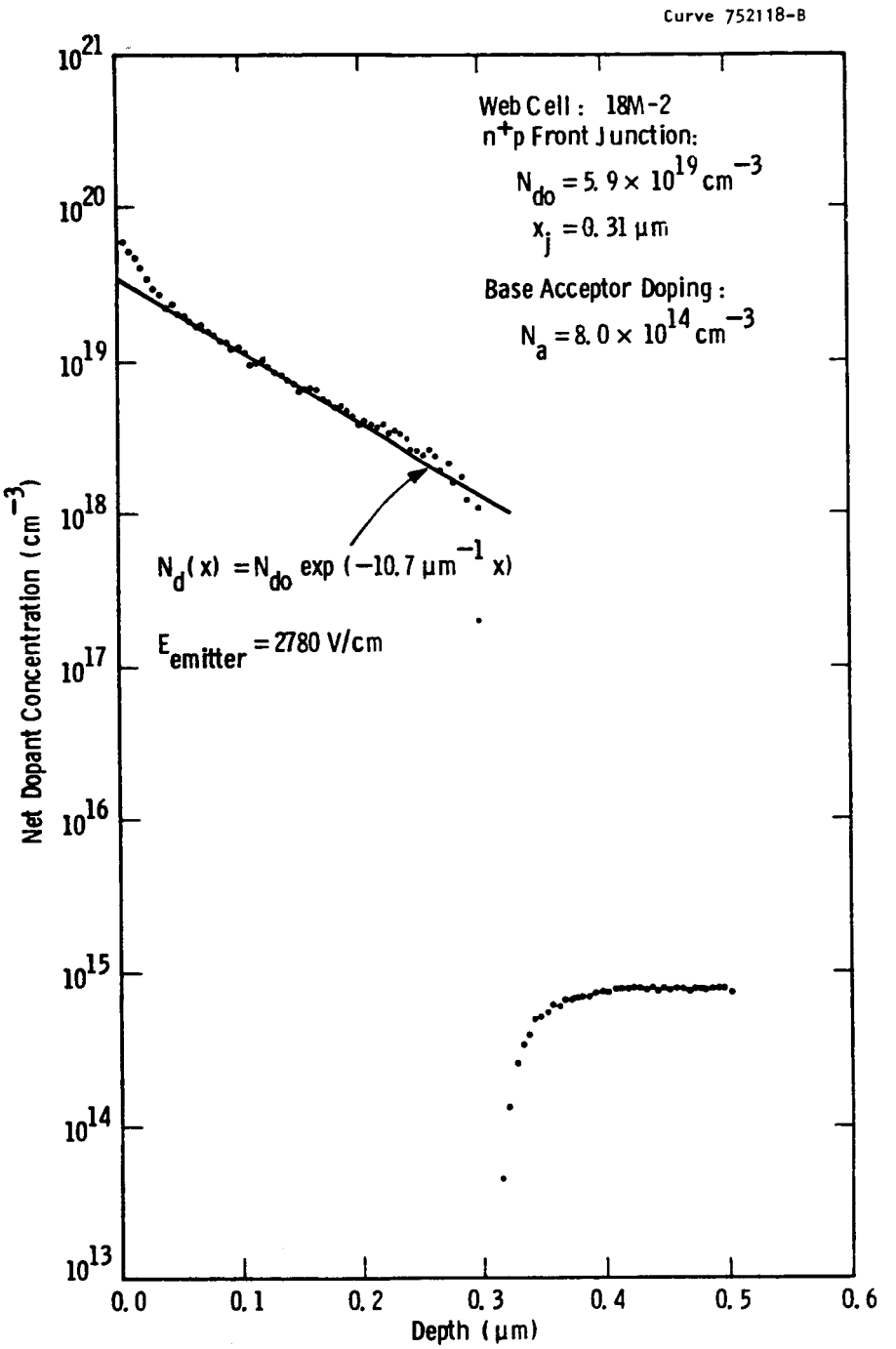

Figure 22 — Dopant profile for the front (n^+p) junction of web cell 18M-2 from Run Cell-3 by spreading resistance. Note exponential decrease in n-type (phosphorus) dopant concentration.

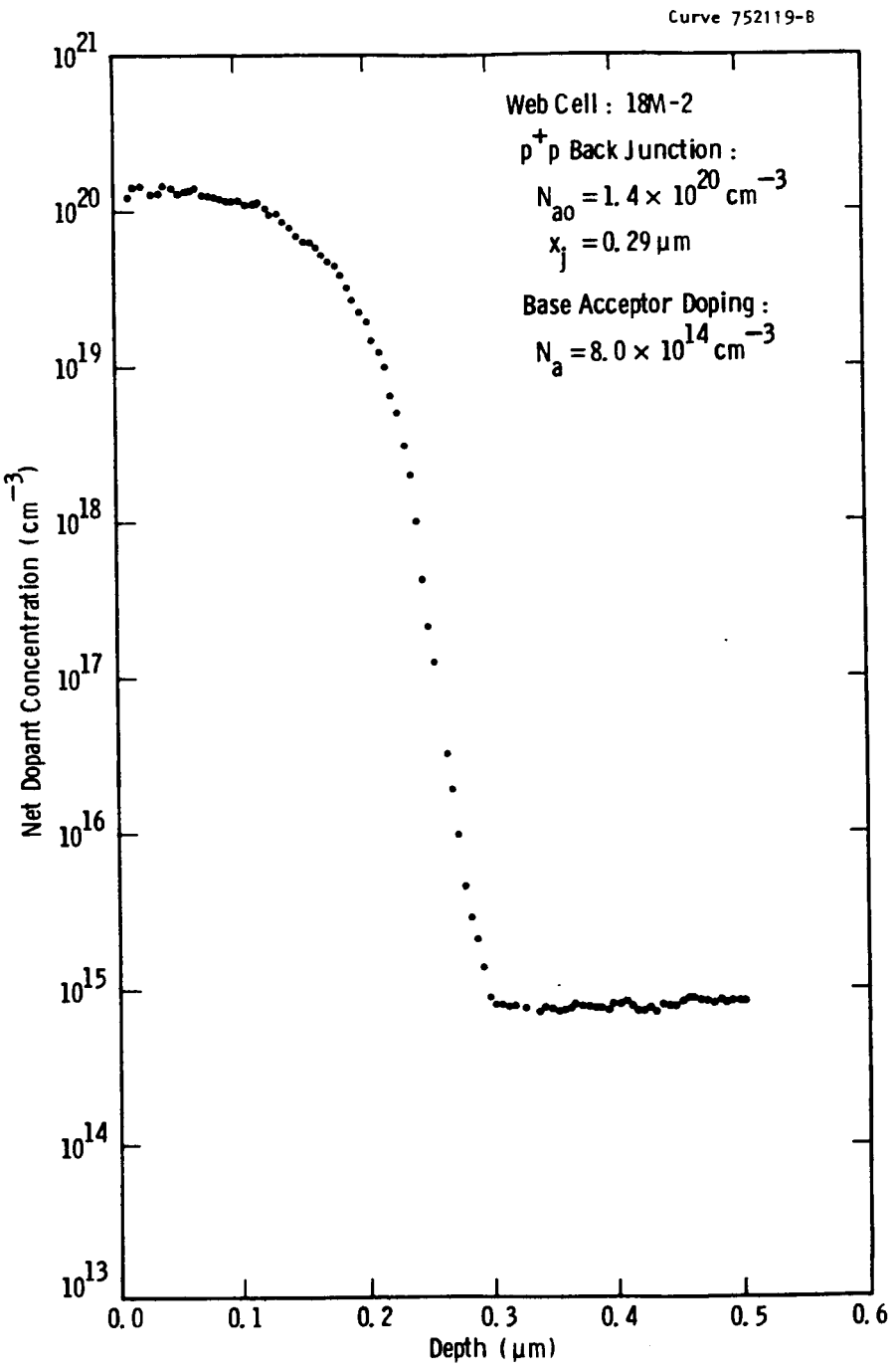

Figure 23 — Dopant profile for the back (p^+p) region of web cell 18M-2 from Run Cell-3 by spreading resistance. Note nearly constant boron concentration near the surface.

Since the profile is exponential, a constant electric field is created within the emitter region having a magnitude of 2780 V/cm and a direction pointing from emitter to base. This drift field, created by the variation in doping density in the emitter, assists the minority carrier holes in the emitter in moving toward the junction for collection. The values that are calculated suggest that the electric field is strong enough to significantly aid in the collection of holes. The existence of this electric field may be an important reason for the high quantum efficiency values at the short wavelengths, as discussed in Section 3.3.3.

The velocity (v_d) with which holes drift in the emitter as a result of this field is given by:

$$v_d = \mu_p E \tag{2}$$

where μ_p is the hole mobility and E is the electric field strength. With μ_p = 60 cm^2/sec (appropriate for a doping density of 10^{19} cm^{-3}) and E = 2780 V/cm, the drift velocity is calculated from Equation 2 as 1.67×10^5 cm/sec.

The time (t) required for a hole to traverse the full width of the emitter region is:

$$t = x_j / v_d \tag{3}$$

where x_j is the junction depth. With x_j of 0.3 μm, t is calculated as 1.80×10^{-10} sec. This is a short time for the hole to spend in the emitter and should be compared with the lifetime of the hole.

Taking the doping density to be 1×10^{19} cm^{-3}, the measured lifetime of holes by the Auger recombination process is 3×10^{-8} sec.[7] This is more that 100 times as long as the computed transit time for

holes to drift across the full width of the base (1.80×10^{-10} sec). The holes therefore appear to be able to be transported to the collecting junction by drift in a time which is short in comparison with the lifetime. Note also that v_d (1.67×10^5 cm/sec) is at least 100 times as large as a typical surface recombination velocity for a passivated surface (1×10^3 cm/sec). This suggests that the hole is moved by the drift field much faster than it diffuses into the front surface where it recombines.

It appears that this drift field may be largely responsible for the good collection efficiency of holes created by the absorption of short-wavelength photons in the emitter. If so, it is fortuitous that the $POCl_3$ diffusion gives rise to such a drift field, for it is not intentionally designed to do so. Additional emitter dopant profiles will be measured in the future to verify that a drift field in the emitter contributes significantly to high short-wavelength response.

4. PROGRAM STATUS

4.1 PRESENT STATUS

The current milestone chart for this program is shown in Table 4. The major conclusions or observations that have been made during this reporting period are:

1. Previous observations that high cell efficiency is related to the absence of dislocations and impurity precipitates, and that twin boundaries are electrically benign, have been confirmed for cell 21B.

2. The termination point in a web crystal appears to be associated with the movement of the heavily twinned region to the external surface of the web, as indicated by cells 8B and 17B.

3. Hydrogen ion implantation (1500 eV, 2 mA/cm^2 for 2 minutes) into web strips after both boron and phosphorus diffusion steps is quite effective in improving minority carrier diffusion length and cell efficiency for web material which is not of superior quality to begin with; this has been clearly demonstrated for cells with small area (1 cm^2), but additional work is needed for full-sized (24.5 cm^2) cells.

4. Web cells with an area of 4 cm^2 have been fabricated with efficiency values up to 16.5% and minority carrier lifetime values up to 38 μs.

5. A double-layer antireflective coating consisting of layers of ZnS and MgF_2 has been optimized for use with silicon substrates having a passivating oxide layer.

Table 4 — Milestone Chart

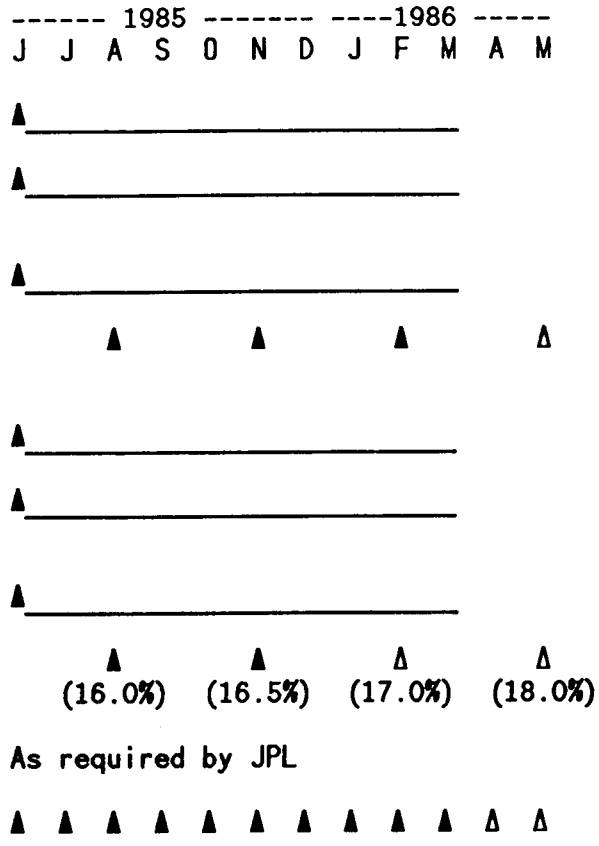

6. A strong drift field (2780 V/cm) in the emitter has been deduced from the dopant profile; this drift field appears to play a significant role in obtaining the high quantum efficiency observed at the low wavelengths (80% at 0.4 μm).

4.2 FUTURE ACTIVITY

Hydrogen ion implantation will be incorporated into the processing of low-resistivity (0.2 ohm-cm) web cells in order to improve the web diffusion length to 100 μm or more in the low resistivity cells. If this is successful, then the properties of web silicon may approach those of low-resistivity float zone silicon. It may then be possible to achieve cell efficiencies exceeding 18% for web cells, as has already been done for float zone cells. An arsenic solid diffusion source will be investigated for obtaining emitters which are doped only to a level of 1×10^{19} cm^{-3} or below. This is expected to reduce the Auger recombination activity in the emitter and thereby increase J_{sc} and V_{oc}.

5. REFERENCES

1. D. L. Meier, A. Rohatgi, T. W. O'Keeffe, P. Rai-Choudhury, R. B. Campbell, and S. Mahajan, "Twin Plane Effects in Dendritic Web Silicon," Proceedings of the 18th IEEE Photovoltaic Specialists Conference, IEEE Catalog No. 85CH2208-7, New York, NY (October 1985), p. 596.

2. J. M. Hwang, D. K. Schroder, and A. M. Goodman, "Recombination Lifetime in Oxygen-Precipitated Silicon," IEEE Electron Device Letters, EDL-7, 172 (1986).

3. K. Holzlein, G. Pensl, M. Schulz, and N. M. Johnson, "Hydogenation of the 'New Oxygen Donor' Traps in Silicon," Appl. Phys. Lett., 48, 916 (1986).

4. D. L. Meier, J. Greggi, R. B. Campbell, and P. Rai-Choudhury, "Development of High-Efficiency Solar Cells on Silicon Web," 6th Quarterly Progress Report for JPL Contract 956786, DOE/JPL-956786/85/6, Westinghouse R&D Document Number 85-9F4-HIWEB-R4, p. 39 (October 1985).

5. S. C. Choo and R. G. Mazur, "Open Circuit Voltage Decay Behavior of Junction Devices," Solid-State Electronics, 13, 553 (1970).

6. A. R. Moore, "Carrier Lifetime in Photovoltaic Solar Concentrator Cells by Small-Signal Open-Circuit Decay Method," RCA Review, 40, 549 (1980).

7. D. Huber, A. Bachmeier, R. Wahlich, and H. Herzer, "Minority Carrier Diffusion Length and Doping Density in Nondegenerate Silicon," Proceedings of the Fifth International Symposium on Silicon Materials Science and Technology, Semiconductor Silicon 1986, Volume 86-4, Electrochemical Society, Pennington NJ.

6. ACKNOWLEDGMENTS

The authors gratefully acknowledge C. W. Hughes for preparing the TEM samples; J. Spitznagel for making available the hydrogen ion implantation system; W. C. Chalmers for implanting the web cells; R. B. Campbell of Westinghouse AESD for supplying the web cells; J. B. McNally, L. E. Hohn, F. S. Youngk, P. Palaschak, and R. J. Fiedor for processing and measurement of the solar cells; B. A. Blankenship for the evaporation of the antireflective coatings; and G. S. Law for document preparation.

FLAT PLATE SOLAR ARRAY PROJECT

Contractor Quarterly, Annual, Interim, and Final
Report Distribution List

Distribution List #645 - Materials & Devices Area
(Total = 37 Copies)

	No. of copies
Applied Solar Energy Corporation Attn: D. C. Leung 15251 East Don Julian Road City of Industry, CA 91746	1
Electric Power Research Institute Attn: E. A. De Meo 3412 Hillview Avenue P. O. Box 10412 Palo Alto, CA 94304	1
Jet Propulsion Laboratory Attn: (Contract Negotiator) M/S 511-303 4800 Oak Grove Drive Pasadena, CA 91109	1
Jet Propulsion Laboratory Attn: Solar Data Library M/S 502-414 4800 Oak Grove Drive Pasadena, CA 91109	15
Jet Propuslion Laboratory Technology Utilization Attn: L. P. Speck M/S 180-302 4800 Oak Grove Drive Pasadena, CA 91109	1
Materials Research, Inc. Attn: Dr. Ram Natesh 790 East 700 South Centerville, UT 84014	1
NASA Headquarters Solar Terr. Systems Div. Attn: Donald Calahan 600 Independence Ave., SW Washington, DC 20546	1
NASA Headquarters Attn: J. P. Mullin, Code RP-6 M/S B636 Washington, DC 20546	1
Research Triangle Institute Center for Semiconductor Research Attn: M. F. Lamorte P.O. Box 12194 Research Triangle Park, NC 27709	1
C. T. Sah Associates Attn: Dr. C. T. Sah 403 Pond Ridge Lane Urbana, Il 61801	1
Solar Energy Research Institute Attn: SEIC/LIBRARY 1617 Cole Blvd. Golden, CO 80401	1
Solar Energy Research Institute Photovoltaic Program Office Attn: Dr. Tom Surek 1617 Cole Boulevard Golden, CO 80401	1
University of Florida Attn: F. A. Lindholm 219 Ginter Hall Gainsville, FL 32611	1
University of Pennsylvania Attn: Prof. Martin Wolf 308 Moore D2 Philadelphia, PA 19174	1
University of Washington Joint Center for Graduate Study Attn: Dr. L. C. Olsen 100 Sprout Road Richland, Washington 99352	1

	No. of copies
U. S. Department of Energy Forrestal Building Attn: R. H. Annan 1000 Independence Ave., SW Washington, DC 20585	1
U. S. Department of Energy Forrestal Building Attn: Dr. Morton Prince M/S 5G026 Photovoltaic Energy Systems 1000 Independence Ave., SW Washington, DC 20585	1
U. S. Department of Energy Forrestal Building Attn: Anthony Scolaro Photovoltaic Energy Systems 1000 Independence Ave., SW Washington, DC 20585	1
U. S. Department of Energy Technical Information Center Attn: Doc. Control & Eval. Branch P. O. Box 62 Oak Ridge, TN 37830	2 + Repro
Westinghouse Electric Corporation Research Laboratories Attn: Dr. P. Rai-Choudhury 1310 Beulah Road Pittsburgh, PA 15235	1
Westinghouse Electric Corporation Research Laboratories Attn: D. L. Meier 1310 Beulah Road Pittsburgh, PA 15235	1